Assessing raindrop evolution over northern Western Ghat from stable isotope signature of rain and vapour

Sheena Sunil Nimya [1,2], Sundara Pandian Rajaveni[1], Saikat Sengupta[1*], Sourendra Kumar Bhattacharya[3], Nandhini Ananthvel[1]

[1]Center for Climate Change Research, Indian Institute of Tropical Meteorology, Ministry of Earth Sciences, Pune-411008, India
[2]Department of Earth, Atmospheric and Planetary Sciences, Purdue University, West Lafayette, IN, USA
[3] Institute of Earth Sciences, Academia Sinica, Taipei 11529, Taiwan
*Correspondence: Saikat Sengupta (saikat@tropmet.res.in)

Abstract

Stable isotopes of hydrogen and oxygen were ~~analysed~~analyzed in rain and vapour samples collected simultaneously from Pune, India, during the 2019 summer monsoon. The ~~heavy isotopes of both oxygen and hydrogen (~~$\delta^{18}O$ and δD~~)~~ were significantly depleted in four events when the Outgoing Longwave Radiation showed a strong negative anomaly, suggestive of large-scale convection. The $\delta^{18}O$ of the rain samples are negatively correlated with their d-excess, indicative of modification of raindrops by evaporation. Analysis of the isotope data indicates isotope exchange between rain and ambient vapour and ~~significant~~ associated raindrop evaporation in the sub-cloud layer. Using the ~~The data plotted in terms of~~ $\Delta\delta-\Delta d$ diagram method of assessing sub-cloud rain and vapour exchange,~~, where Δ indicates the difference between rain equilibrated vapour and the surface vapour, show an equal number of points lying in the 3rd and 4th quadrants, suggesting an equal share of two effects:~~ our data suggest an equal share of equilibrium exchange ~~with ambient vapour~~ and drop evaporation.

We used a one-dimensional Below Cloud Interaction Model to quantify sub-cloud processes affecting raindrop evolution. A Rayleigh ascent assumption in BCIM ~~overestimates~~ simulations yield higher rain isotope values, although model and observed values are well correlated. Using radiosonde-based temperature and humidity profiles and constructing vapour isotope profiles from a combination of satellite (Tropospheric Emission Spectrometer) data and a global circulation model (LMDZ) output, simulations improve ~~and good~~the agreement of the model with observed values~~ is obtained~~. Sensitivity studies reveal that model ~~outputs~~ values are strongly influenced by vapour isotope ~~profiles~~ratios, and moderately by drop size, temperature and relative humidity. Raindrop evaporation estimated from mass change in the model shows that, on daily scale, the drop evaporation varies from 4% to 6~~0~~1% and, on average, 23~~-~~% of the drop mass evaporated in this region. It is seen that the raindrop evaporation reduces the rainfall, especially in the lower range of precipitation. The evaporation also influences the heat budget affecting monsoon convection.

1. Introduction

The Intergovernmental Panel on Climate Change (IPCC) has emphasized the importance of recycled moisture in the atmosphere (IPCC, 2014). Moisture recycling includes processes by which a fraction of the precipitated water returns to the atmosphere and cause further precipitation over the same area (Gray, 2012). These processes are soil evaporation, transpiration from plants, intercepted or condensed water on leaves, and evaporation from falling raindrops (Brubaker et al., 1993; Trenberth, 1999). Thise ~~moisture~~ recycling increases with ambient temperature but decreases with ~~increasing~~ humidity (Pranindita et al., 2022; Zaitchik et al., 2006; Zhang et al., 2021). It has been seen (Kumar et al., 2021; Pathak et al., 2014) that a high precipitation recycling ratio (~15%) pertains~~operates~~ over India during the Indian Summer Monsoon (ISM; June-September). Among the influencing ~~recycled moisture sources~~factors, raindrop evaporation is difficult to estimate because ~~(1)~~ the parameters needed for estimating rain evaporation are not accurately available from satellite sources, ~~and (2) station-based meteorological observations using Micro rain radars are limited (Dai et al., 2019; Li and Srivastava, 2001; Xie et al., 2016).~~

Stable isotopologues ($^{1}H_2{}^{18}O$, $^{1}H^{2}H^{16}O$, $^{1}H_2{}^{16}O$) of ~~liquid precipitation samples~~rain waters can be used to assess the magnitude of raindrop evaporation (Crawford et al., 2017; Rahul et al., 2016; Salamalikis et al., 2016; Wang et al., 2021; Xiao et al., 2021). Falling raindrops exchange isotopes with the ambient vapour; this happens throughout the fall but occurs mostly in the unsaturated sub-cloud layer. The magnitude of this exchange, which alters the rain isotope ratios, can~~, in principle,~~ be used to quantify the extent of raindrop evaporation. Using satellite-based observations of vapour isotopologues ($^{1}H^{2}H^{16}O$ and $^{1}H_2{}^{16}O$) and an isotope mass balance model, Worden et al. (2007) estimated that in the tropics, ~~during the October to March interval,~~ nearly 20 % of the mass of raindrops evaporates. However, they noted that the satellite data has limited temporal and spatial coverage. Therefore, estimating drop evaporation on a daily to monthly scale is difficult. Raindrop evaporation has also been estimated from ground-based rain isotope observations and a set of empirical equations (Froehlich et al., 2008; Li et al., 2021; Wang et al., 2016; Zhu et al., 2021). However, it ~~remains~~ is a challenge to account for all cloud microphysical processes and their associated isotopic fractionations. Normally, these processes are considered for simulating rain isotope values in various General Circulation Models (GCM; Risi et al., 2019; Yoshimura et al., 2008; Stewart, 1975). But~~However,~~ recent studies have shown that most of these GCMs ~~over or underestimate~~fail to estimate raindrop evaporation correctly in tropical India (Nimya et al., 2022; Sengupta et al., 2023). This is possibly due to the coarseness of grid sizes used in these GCMs, which are inadequate to capture the region-specific complexities of processes controlling the evaporation. This necessitates controlled isotope observations and region-specific models for ~~a reasonable~~proper estimation of this parameter (Aemisegger et al., 2015).

Various approaches have been followed to estimate raindrop evaporation using paired observations of rain and vapour isotopes. For example, a bin resolved microphysical model was used to quantify drop evaporation during the Atlantic Tradewind Ocean–Atmosphere Mesoscale Interaction Campaign (ATOMIC; Sarkar et al., 2023). Graf et al. (2019), based on surface rain and vapour isotope observations in Zurich,

Switzerland, ~~provided a rationale to evaluate various processes controlling the isotope values. They~~ developed a simple one-dimensional model (Below Cloud Interaction Model, BCIM) which considers ~~essential~~ various cloud microphysical processes during raindrop formation (condensation, vapour deposition, riming, etc.) as well as evaporative exchange processes within and below the cloud. This model simulates the isotopic evolution of an ice/liquid drop as it undergoes exchange processes while falling to the ground. ~~That model determines the isotopic evolution of an ice/liquid drop released from a desired altitude and undergoing exchange processes enroute its fall to the ground.~~ However, being a one-dimensional vertical model, it does not consider any moisture advection, updraft and downdraft. ~~Nevertheless, it is worthwhile exploring the efficacy of that model in a semi-tropical region like Pune during the ISM when advected moisture fluxes play an important role (Levine and Turner, 2012).~~

In the tropical Western Ghat (WG) region of India, shallow convective clouds ~~predominate~~ are the dominant types (80 % of clouds occur below 4 km and 45 % below 2.5 km altitude) during the ISM (Konwar et al., 2014). Faster evaporation of smaller raindrops associated with intense rainfalls from these clouds provides significant positive energy feedback to form mesoscale convection (Konwar et al., 2014; Tao et al., 2012). A study of drop size distributions showed that raindrop evaporation prevails in the warm rain process occurring in this region (Murali Krishna et al., 2021). The current study investigates the applicability of the BCIM to predict rain isotopes and rain drop evaporation in ~~a tropical Indian~~Pune ~~region using~~, situated on the lee side of the WG using paired observations of rain and vapour isotopes ~~for a summer monsoon~~during ISM ~~season~~.

2. Experimental Methodology

2.1 Study area

Rainwater and vapour samples were collected from the ground level at the Indian Institute of Tropical Meteorology (18.53° N, 73.85° E), Pune during the summer monsoon of 2019. This region receives >90 % rainfall during the ISM and is situated at the lee ~~(rain shadow)~~ side of the Western Ghat m~~M~~ountain (Fig. 1). Rainfall in Western India occurs from mid-tropospheric low-pressure systems in several episodes, each of which usually lasts for 2–3 days. These systems are locked in place during these periods and fed by moisture derived from the Arabian Sea (Wang et al., 2006; Rao, 1976). The geographic location of the region, its altitude, rainfall variation across the WG mountains, and the topographic profile across Pune are shown in Fig. 1. There is a sharp variation of rainfall across the mountain from the coastal zone (30 mm day^{-1}) to the lee side (12 mm day^{-1}) which is a characteristic of orography-induced rainfall (Fig. 1). The surface air temperature in Pune varies from 20° C to 30° C during the ISM (Pattanaik et al., 2019).

Formatted: Font: Not Bold

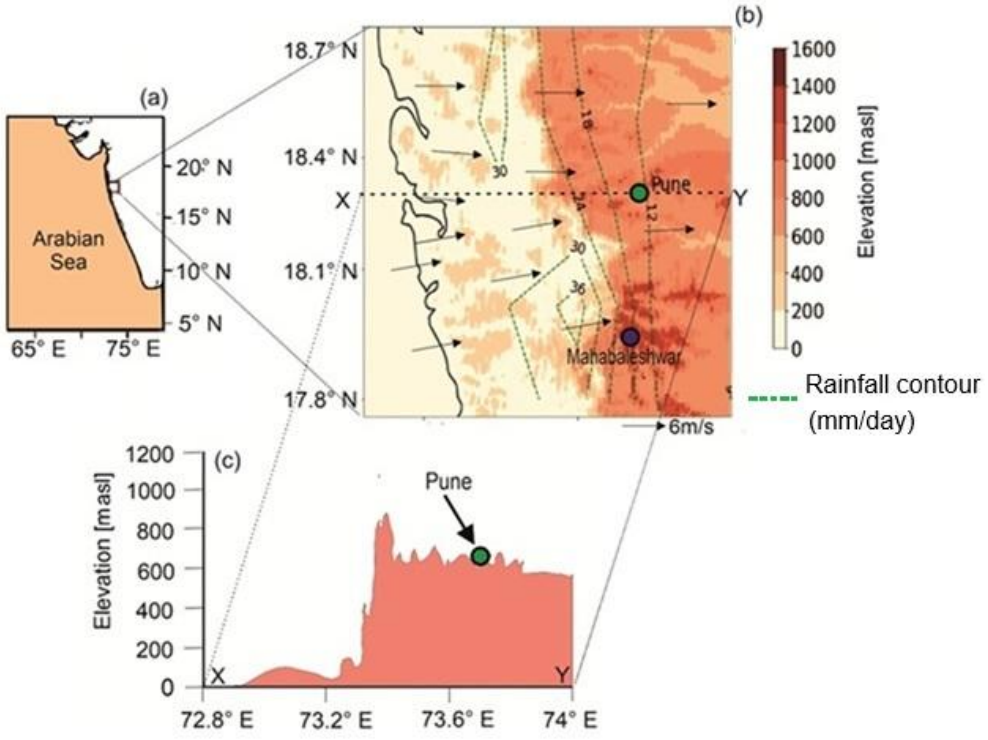

Figure 1. (a) The location of the study area in India. **(b)** Topographic map of the northern Western Ghat, India (prepared based on the GTOPO30 digital elevation model). The rainfall contours (long-term ~~(1901-2017)~~ mean June-September rainfall in mm/day) were constructed using gridded (0.25°x0.25°) rainfall data (1901-2020) from the India Meteorological Department (IMD). **(c)** A topographic profile along the latitude 18.53° N through Pune (Green circle at an altitude of 560 m) shows its position.

2.2 Sample Collection, Isotope Measurements

The onset and withdrawal dates of ISM (based on wind direction, specific humidity, and outgoing long wave radiation, OLR; IMD, 2019) at Pune in 2019 were 22 June 2019 and 4 October 2019, respectively. ~~Liquid~~ Rain water samples were collected during ~~rains~~ 2019 monsoon using samplers made following the guidelines of the International Atomic Energy Agency (see Supplementary Information Fig. S1-1). For vapour samples, an in-house fabricated glass condenser was used (see Fig. S2-1). ~~Most of the~~Twentynine vapour samples were collected during the rainy days along with rain samples (avoiding direct raindrop entry), ~~but some~~and fourteen ~~were also~~samples were collected during ~~the~~ non-rainy days~~period~~. The vapour collection efficiency was estimated from the amount collected against the amount expected (see Table S2-1). Due to logistical problems, vapour samples could not be collected before mid-July. ~~A total of 50 vapour samples were collected and 29 of them coincided with the rain sampling days.~~

The samples (rain water and condensed vapour) were measured using a Liquid Water Isotope Analyser (Model Number TIWA-45-EP, Los Gatos Research). This instrument measures liquid samples using Off-Axis integrated cavity output spectroscopy (OA-ICOS) with a routine precision of 0.1 ‰ and 1 ‰ for $\delta^{18}O$ and δD

(relative to VSMOW) respectively (Rajaveni et al., 2024; see also Supplementary Information SI-3). The d-excess values defined as: d-excess = $\delta D - 8*\delta^{18}O$ (Dansgaard, 2012) have a precision of 1 ‰. The reported ~~daily~~ rain isotope data are given after being weighted by the amount of rainfall on that day.

2.3 ~~Satellite and g~~Ground-based meteorological ~~data~~, Radiosonde and Satellite data

The rainfall data are obtained from the Pune observatories of the IMD, available at the National Data Centre (www.imdpune.gov.in/ndc_new/ndc_index.html). Apart from rainfall, daily average temperature and relative humidity data for the Pune observatory were also obtained. The daily gridded data (zonal and meridional wind, specific humidity, air temperature, and cloud liquid water content) from the European Centre for Medium-Range Weather Forecasts Reanalysis (ERA5) dataset with a resolution of 0.25° × 0.25° (Hersbach et al., 2020) and the Interpolated Outgoing Longwave Radiation (OLR) data (2.5° × 2.5°) from NOAA (https://psl.noaa.gov/data/gridded/data.olrcdr.interp.html) are used in this study.

The upper-air radiosonde measurements (relative humidity, temperature) carried out over Pune were obtained from the University of Wyoming repository (http://weather.uwyo.edu/upperair/sounding.html). ~~–~~The ~~vertical variation~~values at ~~(~~ every 50 mb interval (about 470 m in height) of the two parameters were~~as~~ available for two times: at 00 UTC and 12 UTC~~, and~~. ~~F~~For our use on daily scale, ~~each parameter,~~ the two profiles for each parameter are averaged to make a representative daily profile. ~~The typical uncertainty of temperature and relative humidity is 0.3° C (Sapucci et al, 2005; Jensen et al., 2016) and 8 % (Xu et al., 2023), respectively.~~ Since the input for BCIM is required at every 1-meter interval a linear interpolation between two consecutive pressure levels in logarithmic scale (Ingleby et al., 2016) was carried out. However, the zone between the cloud base (lifting condensation level LCL) and the drop introduction height (taken as the cloud liquid water content CLWC peak) poses a problem. As the BCIM requires RH=100% for the formation of water droplets, the RH values above the LCL and up to the CLWC peak were considered as 100% disregarding the radiosonde data above the LCL (see section 2.4.2 and SI-8b). The typical uncertainty of temperature and relative humidity is 0.3° C (Sapucci et al, 2005; Jensen et al., 2016) and 8 % (Xu et al., 2023) respectively.

Tropospheric Emission Spectrometer (TES) Level 2 (Nadir-Lite-Version 6) retrievals of HDO and H_2O profiles for the available period (2005–2007) are used to construct mean vapour δD profiles. The details of quality control criteria and biases associated with TES observations are discussed by Herman et al. (2014) and Worden et al. (2011). Grid point observations of δD by TES have a precision of ~ 10–15 ‰, which reduces to 1–2 ‰ when the data are averaged over a larger region (Lee et al., 2011; Pradhan et al., 2019).

To decipher the moisture sources for vapour/rain at and around our study area, 48-hour air mass back trajectory analysis was carried out at 850 mb pressure level using the NOAA Hybrid Single-Particle Lagrangian Integrated Trajectory (HYSPLIT) model (Draxler and Hess, 1997). The model tracks the movement of air parcels backward from a given location for a desired period (see SI-4).

2.4 The input parameters for BCIM

To quantify the sub-cloud processes altering the rain isotope values, we used the Below Cloud Interaction Model BCIM (Graf et al., 2019). ~~Various parameterisation schemes used in the BCIM have been discussed by Graf et al.(2019).~~ A brief description of this model, as applicable for the shallow cloud processes

Formatted: Not Highlight
Formatted: Not Highlight
Formatted: Not Highlight
Formatted: Not Highlight
Formatted: Not Highlight
Formatted: Not Highlight
Formatted: Not Highlight
Formatted: Not Highlight
Formatted: Not Highlight
Field Code Changed
Field Code Changed
Formatted: Highlight

over Pune, is provided here. The model comprises a single vertical column that extends from the ground level to the point at which a single hydrometeor is introduced. Within this column, the hydrometeor descends under the influence of gravity, undergoes growth or evaporation (depending upon the ambient humidity and temperature), changes its isotopic composition through equilibrium and kinetic isotope exchange with surrounding vapour, and finally reaches the surface as raindrop. The final isotopic composition of the ~~hydrometeor~~ drop is estimated following four steps of calculations: (1) setting up the initial condition involving the drop introduction height and its size, (2) estimation of the initial isotopic composition of the hydrometeor, (3) tracking the ~~microphysics~~ microphysical evolution of a falling hydrometeor, and (4) tracking the changes in isotopic composition of the hydrometeor along the descent. For these calculations, the model requires altitude profiles of temperature (T)~~-~~, relative humidity and vapour isotopes ~~altitude profiles~~ for a given day as input parameters. The drop is assumed to form in equilibrium (at relative humidity, RH=100 %) at a level which differs from day to day. The input parameters for the vapour can be introduced into the BCIM in two different ways: (1) the profiles can be calculated based on assumption of idealised (moist) adiabatic ascent of an air parcel from the surface to the top of the column following a Rayleigh model; RH, T and isotope values at various pressure levels are then estimated from the Rayleigh distillation equations starting from the measured surface values or (2) the pressure level specific values of RH and T from radiosondes and isotope values from satellite data and/or any model.

Since our aim is to understand the isotopic modification and mass loss suffered by the drops on the way down, we introduce here two parameters ~~Δδ and Δd~~ expressing the deviation of the final rain composition at the ground from the ambient surface vapour (Graf et al. 2019). ~~For this, we use~~This is most clearly expressed by the difference between the isotopic composition of vapour in equilibrium with the rain samples (rain eq. vapour) and the ambient surface vapour ~~and~~ defined as: $\Delta\delta$ = δD (rain eq. vapour) - δD (surface vapour) and similarly for d-excess, Δd = d-excess (rain eq. vapour) - d-excess (surface vapour).

Formatted: Indent: First line: 1.27 cm

2.4.1 Drop size assignment

The model also requires the input diameter of the initial hydrometeor. Unfortunately, no disdrometer or Micro Rain Radar observations are available for Pune during 2019. We, therefore, adopted ~~an empirical procedure, known as the~~ the well-known Marshall-Palmer ~~(M-P distribution)~~ distribution~~relationship~~ (Marshall and Palmer, 1948), to estimate the mean drop size at the ground. First, we estimated the hourly mean drop size of the raindrops ~~at the ground level~~ from the hourly rain rate data, available from the IMD observatory at Shivajinagar, Pune, located about 4 km away from the sampling location. Next, we calculated the 24-hour mean drop size by taking a weighted average of the size using rain rates as the weights. The calculated drop sizes at the ground vary from 0.61 to 1.80 mm for various days. The drop diameter at the ground is next provided as an input and the ~~initial~~ drop size at the drop introduction height (about 2.0 km above ground) is estimated iteratively in BCIM using the microphysics part of the model~~., using the temperature and RH profiles.~~ This procedure was adopted for each day. The accuracy of the drop size based on the M-P distribution and the rain rate is limited, but this was the only ~~imperative~~ option ~~since no drop size (disdrometer) measurements were available~~ available to us. Our choice was guided by earlier modelling and observational studies where the M-P distribution was used (Graf et al., 2019; Sarkar et al., 2023; Morrison et al., 2020; Ryu et al., 2025; Jiang et al., 2024).

2.4.2 Drop formation height assignment

In a simplified picture, ~~T~~the formation height of the drop should be fixed by considering the most probable altitude range where the majority of the drops exist on any given day. This i~~was~~ not known a priori and was inferred from the cloud liquid water content (CLWC) analysis. The CLWC is defined as the total mass of liquid water droplets suspended in a unit volume of air within a cloud, typically expressed in grams per cubic meter or per kilogram of dry air .An earlier study by Kumar et al. (2014) showed that a peak of Cloud Liquid Water Content ~~(CLWC)~~ is often present at about 850 mb during the monsoon season over western India. In the present case, the CLWC data for 29 days of the study period obtained from the ERA5 dataset show a peak at 830±70 mb, i.e., about 1650 m above msl (See Table S5-1 and Fig. S5-1). Here, we consider the CLWC peak of a given day as the drop introduction height for that day.

Clouds comprising small size water droplets form by condensation above a certain base height where the vapour pressure equals the saturation vapour pressure. ~~In the present study, w~~We can consider the cloud base height ~~as~~ to be the Lifting Condensation Level (LCL) where RH attains~~is~~ 100%. The RH and T profiles from the radiosonde data at various heights (with extrapolated ground level values; see SI-8b) are used to estimate the LCL using the Skew T-Log P diagram for all 29 sampling days. The LCL varies from 820 to 900 mb, and the average height is 890 ± 20 mb (about 1050 m; see Table S5-1). We notice that the LCL is always below ~~(about 600 m on average)~~ the corresponding day's CLWC peak (by about 600 m on average)~~, as it should be,~~ and therefore, the drop falls through a zone of 100% RH till it emerges below the cloud base at~~or~~ LCL (see SI-5) where it falls down through a region of RH less than 100%.

~~.~~

2.4.3 Isotopic composition of the ambient vapour and hydrometeor

The isotopic composition of the ambient vapour at various heights is not known a priori. They are estimated from one of several possible sources and vary depending on the inherent assumptions. Three types of profiles were considered in this work to improve the BCIM predictions to match the observed rain isotope results. To clearly present how this was done, we discuss the vapour isotope profiles along with the results for each choice in Results (Section 3.2.1 to 3.2.3 ; Table 1).

The initial composition of the introduced hydrometeor is next calculated by assuming formation in equilibrium from the vapour at this altitude at the ambient temperature. Subsequently, the composition of the falling ~~The isotopic composition of the introduced hydrometeor is estimated by assuming formation in equilibrium from the vapour at this altitude at the ambient temperature. Subsequently, these drops grow or diminish as they fall. The isotopic composition of the falling~~ hydrometeor at lower altitudes is ~~then~~ calculated by using isotope mass balance and diffusive transport associated with exchange with the surrounding vapour involving appropriate fractionation factors (Graf et al., 2019).

~~from the composition of the surrounding vapour by using isotope mass balance and diffusive transport involving appropriate fractionation factors (Graf et al., 2019).~~

The mass and temperature of the hydrometeor are calculated along its fall trajectory using the equations governing the microphysics of the falling hydrometeor (Foote and du Toit, 1969; Pruppacher and Klett, 2010).~~The terminal velocities are estimated using Foote and du Toit (1969). To calculate the change in mass and~~

Formatted: Indent: First line: 1.27 cm

Formatted: Not Highlight

Formatted: Not Highlight

~~temperature between two pressure levels, t~~The temperature, pressure, and relative humidity values are interpolated ~~between these two levels~~from the adopted profiles in various runs. ~~These changes are estimated as per Pruppacher and Klett (2010).~~ It is important to mention here that many processes considered in the original BCIM (e.g., ice formation, vapour deposition, rimming) do not occur for the shallow convective clouds in Pune (Utsav et al., 2017). Therefore, the BCIM inputs are ~~taken accordingly in the present study~~considered only ~~upto~~up to the rain drop introduction altitude (see Table 1). The model also does not consider downdraft or advection of air masses. The inputs for various simulations are obtained from several possible sources given in Table-1 and discussed in Section 3.2.

~~an altitude of 1500m from the surface and hence the model did not consider the processes related to ice formation (e.g. vapour deposition, rimming etc) in our case . The inputs for various simulations are obtained from several possible sources discussed later in Table-1 and Section 3.2.~~

Formatted: Indent: First line: 0 cm

Formatted: Justified, Widow/Orphan control, Tab stops: Not at 1.24 cm

3. Results

We present the results of the current study broadly in two sections: (1) Results of isotope analysis and (2) Results of BCIM simulations. The first section presents the measured isotope ratios in the context of meteorological parameters, whereas the BCIM simulations are compared with the measured values in the second section.

3.1 Results of isotope analysis

Measured rain and vapour isotope ratios ($\delta^{18}O$ and d-excess) on a daily scale are plotted in Fig. 2a and 2b. The general pattern of variations in vapour and rain $\delta^{18}O$ values is similar; both decrease significantly and consistently after mid-August. The vapour δ-values are lower than the rain. In contrast, the d-excess values of vapour are always much higher. The $\delta^{18}O$ and d-excess values of rainwater range from −10.8 ‰ to 1.5 ‰ and −2 ‰ to 12 ‰, respectively, while those of the vapour range from −19 ‰ to −9 ‰ and 10 ‰ to 30 ‰, respectively. The mean and 1σ standard deviation of $\delta^{18}O$ and d-excess values of rainwater are −1.3±2.6 ‰ and 3.9±2.7 ‰, while those of the vapour are -12.5±2.5 ‰ and 18.3 ± 5.2 ‰, respectively. The $\delta^{18}O$ (Fig. 2a) and d-excess (Fig. 2b) time series show four interesting features: (1) For the four date ranges: 27-29 July, 24-27 July, 4-8 September, and 19-27 September, significant and consistent decrease in isotope values are observed in both rain and vapour phases (marked 1, 2, 3, 4 in Fig. 2a; no vapour data available for date range 1), (2) On 19 September, the vapour shows a sudden decrease (marked A in Fig. 2a), (3) there is a gradual decrease in vapour $\delta^{18}O$ values and an increase in d-excess values with the progress of the monsoon, especially ~~more~~prominent in the later part, and (4) rain d-excess values remain constant with time but $\delta^{18}O$ of both rain and vapour start decreasing beginning from early September ~~onwards~~.

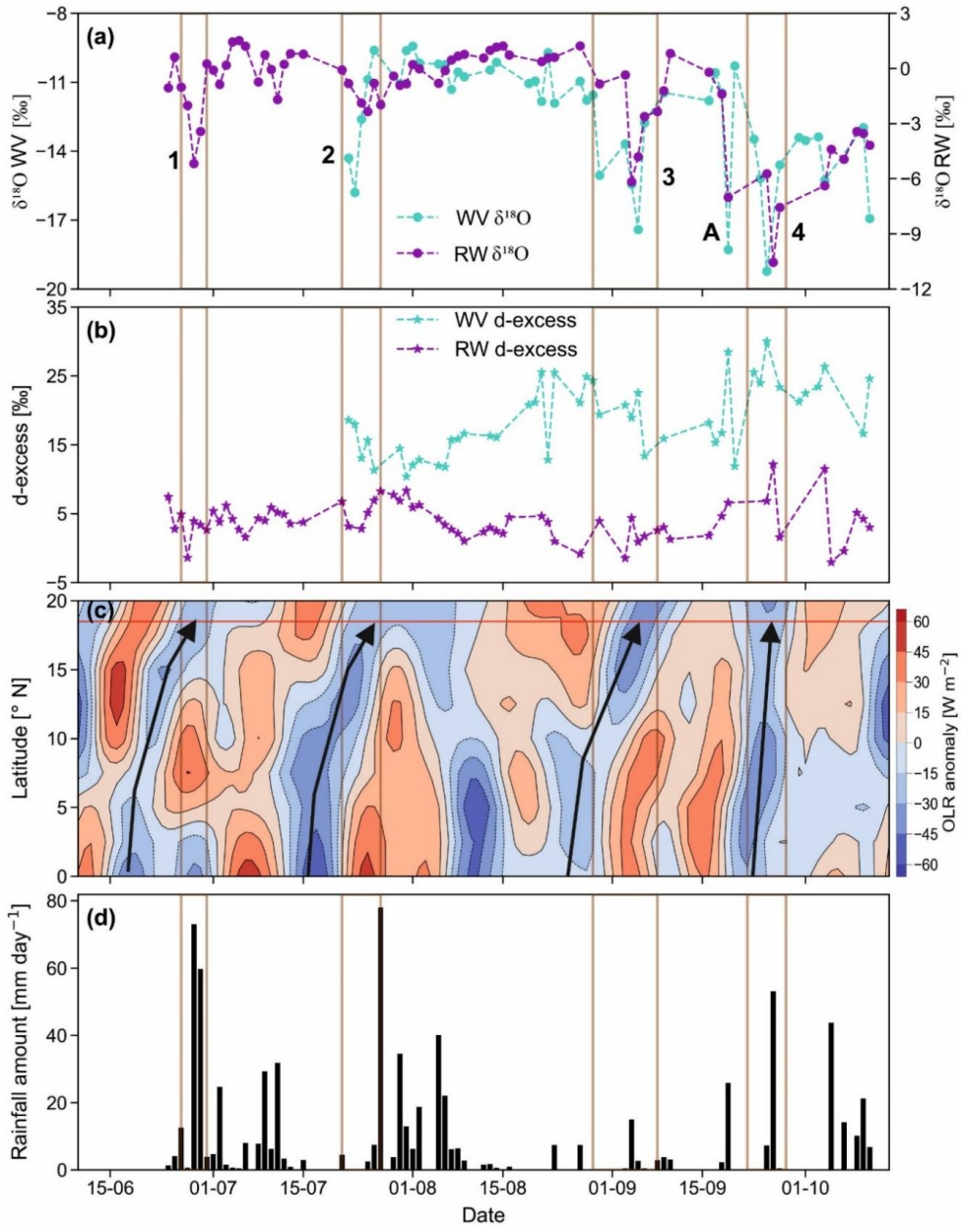

Figure 2. The time series of (a) $\delta^{18}O$ ~~(a)~~ and (b) d excess values, ~~(b)~~ of the rainwater (RW) and water vapour (WV), **(c)** OLR anomaly (W m^{-2}), and **(d)** daily rainfall (mm over 24 h; d) in Pune. The four vertical boxes (numbered 1, 2, 3, and 4) denote synchronous low OLR values and low isotope values (i.e., less than their respective μ-0.5σ values). These periods are defined as low isotope events. The label, A, indicates one isolated low isotope value without low OLR association. Thick arrows show how convective cloud bands (indicated by low OLR anomaly) traverse to the sampling region over Pune from ~~South~~south-west. Note highly depleted values on 19, 25 and 27 September.

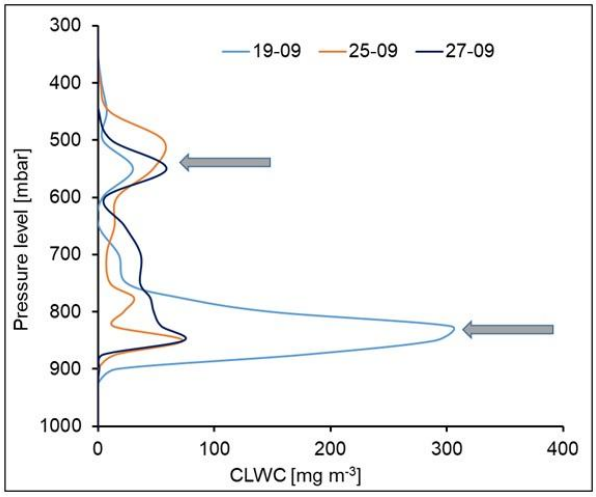

Figure 3. Presence of second CLWC peaks at higher altitudes (about 550 mb) on 19, 25 and 27 September 2019 (beside the first major peaks at lower altitudes) when highly depleted rain $\delta^{18}O$ values were observed in association with negative OLR anomaly (see Fig. 2). The altitudes of the two sets of peaks are shown by two arrows. The data for the plot is from ERA5 ~~dataset is used for this plot~~.

Isotopic depletions in rain and vapour samples in the tropics are often associated with deep convection (Lekshmy et al., 2014; Risi et al., 2008; Sengupta et al., 2020). ~~, whose s~~Signature of such a phenomenon is possibly present here in the ~~present data in the~~ form of depleted-isotope events when isotope ratios of a group of samples fall below the overall mean (μ) minus half the standard deviation (σ) (Sengupta et al., 2020). To find the relation of these events to large convective episodes, a latitude-time Hovmoeller plot of daily OLR anomaly (averaged over the longitude 70° E -75° E) is examined in Fig. 2c. The OLR values are often used as a proxy for convection. Since the cloud top temperatures are an indicator of cloud height, a negative OLR anomaly means colder cloud top temperatures or higher cloud. ~~We define depleted isotope events as those where isotope ratios of a group of samples fall below the overall mean (μ) minus 0.5half the standard deviation (σ) (Sengupta et al., 2020). To examine the extent to which the depleted (more negative) isotope events are related to large convective events, a latitude-time Hovmoeller plot of daily OLR anomaly (averaged over the longitude 70° E - 75° E) is displayed in Fig. 2c. The OLR values are often used as a proxy for convection in tropical and subtropical regions. Since the cloud top temperatures are an indicator of cloud height (colder is higher), a negative OLR anomaly means colder cloud top temperatures or higher cloud~~ thickness. This, in turn, implies extensive coverage by deep cloud systems, characteristic of mesoscale convection ~~and rain~~. A time synchronous association of low OLR and depleted-isotope events thus indicate mesoscale convection affecting isotope values. Fig. 2c indicates four such isotope-depleting mesoscale events (marked as 1, 2, 3 and 4 in Fig. 2a). In addition, we also see one depleted-isotope event without such association (marked as A in Fig. 2a). ~~We also note that~~Interestingly, there were significantly ~~high~~ prominent second CLWC peaks on the three days, 19, 25 and 27 September, at much higher levels (about 550 mbar or about 5.5 km altitude) shown in Fig. 3. ~~(~~corresponding to

the event number 4 mentioned above~~)~~.

~~We note from~~ Fig. 2d shows that major rainfall occurred during the months of July and August; the relative humidity at the surface during the whole monsoon season varied from 71 % to 97 %, and the surface temperature varied from 25° C to 30° C (see Fig. S10-1). It is evident from Fig. 2d that deep convection is associated with high rainfall for the three events 1, 2, and 4. A recent study, based on a year-long continuous measurement of atmospheric vapour in Sri Lanka (a nearby tropical country under similar monsoon system) also found such isotopic depletion during high rainfall events (Wu et al., 2025).

Fig. 4a shows the local meteoric water line (LMWL) using rainwater samples and the local water vapour line (LWVL) using vapour samples from this study. The LMWL equation is $\delta D_r = (7.3\pm0.1)\ \delta^{18}O + (3.0\pm0.3)$ and the LWVL, $\delta D_v = (6.4\pm0.2)\ \delta^{18}O - (1.9\pm3.0)$, subscripts r and v denote rain and vapour. The slope and intercept of the LMWL values are lower than those of the Global Meteoric Water Line (GMWL), which are 8.0 and 10.0, respectively (Dansgaard, 2012; Gat, 1996). This difference, though small, suggests some amount of below-cloud evaporation of the rain~~s~~. At Roorkee, a high-latitude Indian Station, Saranya et al. (2018) found an LMWL with a lower slope (5.4) but a higher intercept (27). They attributed these changes to the contribution of evaporation from water bodies nearby and moisture recycling during the monsoon. Rahul et al. (2016) got a similar slope (7.4) but a lower intercept (1.5) in Bangalore (southern central India, at a high altitude of ~1 km). The lower slopes of meteoric water lines provide a signature of evaporation processes associated with kinetic fractionations occurring during rain.

The d-excess values of rain samples suffering evaporation generally bear a negative relationship with $\delta^{18}O$ values (Bonne et al., 2014; Munksgaard et al., 2020) as~~.~~ ~~This is also~~ seen in our study (Fig. 4b**)** ~~where rain d-excess decreases with an increase in $\delta^{18}O$ values.~~ In addition, the vapour d-excess values also show a statistically significant negative correlation with $\delta^{18}O$ values (Fig. 4b; $R^2 = 0.61$; $p = 0.001$), probably indicating contribution of vapour derived from rain evaporation (Kurita, 2013; Risi et al., 2021). Correlation studies can be indicative, but the causative factors behind the above variations can be explored only with the help of a process-based model like BCIM.

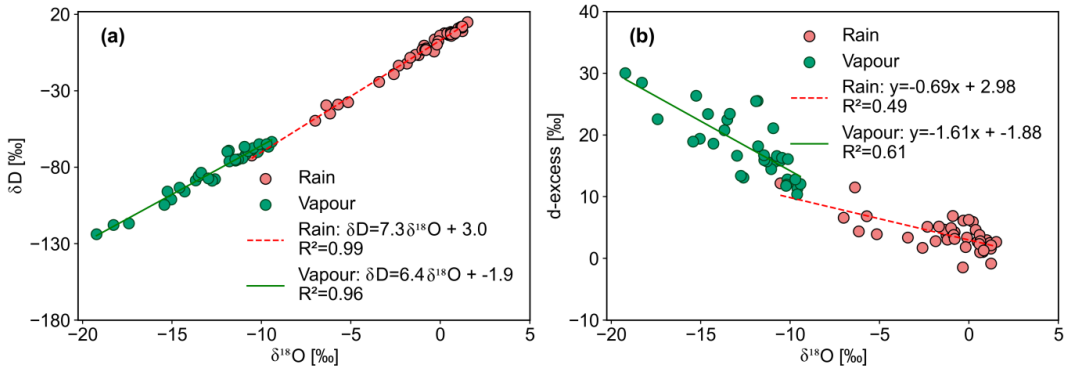

Figure 4. A cross-plot of **(a)** δD and $\delta^{18}O$ of rain and vapour; **(b)** a cross-plot of d-excess and $\delta^{18}O$ of rain and vapour showing anti-correlation. ~~Mean~~ The regression lines and correlation coefficients are shown inside the plots.

3.2 Results of BCIM simulations

As discussed in section 2.4, simulation runs of BCIM were carried out under three assumptions about the vertical profiles of RH, T and vapour isotopes. The results are shown as Run-1, Run-2 and Run-3, which were designed to make progressive improvement in reproducing the measured rain isotope data by altering the input parameters. The sources of input profiles of ambient temperature (T), relative humidity (RH), vapour δDv, and vapour d-excess (dv) required for the three BCIM runs are given in Table 1.

~~**3.2.1 Run-1: Rayleigh ascent**~~

~~The sources of input profiles of ambient temperature (T), relative humidity (RH), vapour δDv, and vapour d-excess (dv) required for three BCIM runs are given in Table 1. In Rayleigh simulations (designated as Run-1), the profiles were calculated using the equations for moist-adiabatic ascent of air parcels (see Appendix A1 of Graf et al.,2019) starting at the surface with values of temperature (T_0)T, relative humidity (h_0)RH, δD_v ($\delta v,0$) and d_v (d-excess of vapour) (dv,0) of each sampling day as inputs. The surface values of δD and d-excess of vapour (denoted by the symbol d) were taken from our vapour measurements along with the daily average temperature and humidity values obtained from the surface observations of IMD (Section 2.3). A dry adiabatic ascent formula is used in the initial phase up to the cloud base (LCL). Above the cloud base, a moist adiabatic lapse rate is used. The dry and moist lapse rates are calculated using equations based on the gravitational constant, specific heat of dry air, mass mixing ratio of vapour, latent heat of evaporation, specific gas constant of dry air, temperature, ratio of specific gas constants of dry air and water vapour, specific humidity and saturation vapour pressure. The input profiles of RH, T, δD_v, and d-excess, for all 29 sampling days are given in Supplementary Information (Fig. S8b-1 and Fig. S8b-2).~~

Table 1. Input parameters for various BCIM runs

Sl. No	BCIM input	Parameters for Run-1	Parameters for Run-2	Parameters for Run-3
1	Drop size	Marshal-Palmer equation using hourly rainfall data obtained from IMD	Same as Run-1	Same as Run-1
2	RH profile	Rayleigh ascent ~15 % increase per km and 100% above CBH to drop introduction height	Radiosonde values normalized to surface observation and changed to 100% above CBH to drop introduction height	Same as Run-2
3	Temperature profile	Rayleigh ascent Lapse rate ~ 5.6°C km^{-1}	Radiosonde normalized to ground value	Same as Run-2
4	δD_{vap} profile	Rayleigh ascent ~7 ‰ decrease per km	TES normalized to measured surface value	δD values reduced slightly (within ±4‰) keeping the shapes like Run-2

Formatted: Subscript

Formatted: Subscript

Formatted: Subscript

Formatted: Subscript

Formatted: Indent: First line: 1.27 cm

5	d-exc$_{vap}$ profile	Rayleigh ascent ~0.1 ‰ increase per km	LMDZ δD and $\delta^{18}O$ values used to get d-exc$_{vap}$ normalized to measured ground value	d-exc$_{vap}$ decreased from Run-2 average of 17‰ to an average ~10‰
6	Rain drop formation height (CLWC peak)	ERA5 Cloud Liquid Water Content peak	Same as Run- 1	Same as Run- 1
7	Cloud Base Height (LCL)	LCL from radiosonde profiles using skew-T log P diagram	Same as Run-1	Same as Run-1

3.2.1 Run-1: Rayleigh ascent results

In Rayleigh simulations (Run-1), the profiles were calculated using the equations for moist-adiabatic ascent of air parcels (following Appendix A1 of Graf et al.,2019) starting at the surface vapour values of T, RH, δD_v and d_v of each sampling day as inputs. The values of δD and d-excess of vapour were taken from our own vapour measurements whereas the daily average temperature and humidity values were obtained from the surface observations of IMD (Section 2.3). A dry adiabatic ascent formula is used up to the cloud base (LCL). Above the cloud base, a moist-adiabatic lapse rate is used. These input profiles for the 29 sampling days are given in Supplementary Information (Fig. S8b-1 and Fig. S8b-2).

Formatted: Indent: First line: 1.27 cm

~~3.2.1.1 Run-1 results~~

Results of Run-1 (Rayleigh ascent) simulations are compared with the observed values of rain δD (Fig. 5a), $\delta^{18}O$ (Fig. 5b), and d-excess (Fig.5c) values. We also construct Δδ–Δd cross plots for both observed and model values in Fig. 5d. Although observed and model isotope values (Fig. 5a and 5b) show strong correlation (R^2=0.86 and 0.79, respectively), the model values ~~are mostly overestimated~~deviate (the plotted points ~~lie below~~deviate from the 1:1 line). The mismatch in e~~over~~stimation~~s~~ of isotopes (for $\delta^{18}O$ and δD) affects the d-excess values considerably more; the points lie far to the right, and no correlation exists between the observed and model d-excess values (Fig. 5c). This is because the d-excess parameter being~~is more sensitive to departure from equilibration~~sensitive, ~~, which means that~~ a small departure in~~of~~ delta values~~ would~~ magnifies~~y~~ the discrepancy in ~~case of~~ d-excess. ~~We also note that m~~Most of the model data points in the Δδ–Δd cross-plot do not agree with the observed data points and lie closer to the origin. ~~However, m~~Many of the model points fall in the lower right quadrant, ~~which is expected in the case of dominant~~indicating presence of strong raindrop evaporation. We also note that the model Δδ and Δd values (Fig. 5d) show smaller variations compared to the observations. The Δδ of the model simulations varies from 0 ‰ to 5 ‰ and Δd from 0 ‰ to -5 ‰, while the observed values have variations of about 25 ‰ (higher by a factor of 5). These comparisons show that the Rayleigh ascent model with the ~~prescribed~~ chosen inputs ~~fails~~fails to reproduce the evolution of the rain isotopes in our region. We suspect that the vertical profiles of RH, T and vapour isotopes need to be modified to improve the simulations. Rayleigh ascent in Run-1 assumes that the source of vapour aloft is an unaltered rising air parcel with constant specific humidity. But we see from Fig. S5-2 and S8b-1 that this condition results in unusually low cloud base over Pune (i.e., the level where RH attains the value of 100%)~~,~~ inconsistent with

observations ~~which is not observed~~ (Naik et al., 2003). In fact, the ERA5 data show that specific humidity decreases with height (Fig. S6-1). It is well known that a decrease in specific humidity is associated with a decrease in ~~the~~ vapour isotope ratios (Noone, 2012; Worden et al., 2007; see SI-6 for details). Moreover, in Run-1, the isotopic inputs for the BCIM isotope lapse rates are taken from the measured surface δD and dexcess. But these vapours are influenced by downdrafts associated with rain events. The downdrafted air brings down vapour with lower isotope ratios contributed by rain evaporation. Therefore, the post-rain values are not representative of the atmospheric column before droplets form, precipitation falls, and rain evaporation occurs. ~~The simulation can possibly be improved if we use RH and T data from local radiosonde observations and try out altogether different isotope profiles having realistic vertical variations.~~

~~–~~To improve the model predictions, we change the profiles as described in the next section.

3.2.2 Run-2 results

~~**: RH and T from Radiosonde and isotope profiles from TES and LMDZ**~~

The failure of Rayleigh ascent method (Run-1) prompted us to explore other sources of vertical profiles of RH, T and vapour isotopes. Instead of Rayleigh ascent method, RH and T profiles are now taken from Radiosonde (section 2.3) and vapour isotope from TES as discussed below. ~~3.2.2.1 RH and T from Radiosonde~~

~~For the study period, the average radiosonde observations were available (see section 2.3) at every 50 mb pressure interval (about 470 m), but the input for BCIM is required at every 1 meter interval. Therefore, a linear interpolation between every two consecutive pressure levels in logarithmic scale (Ingleby et al., 2016) was carried out to obtain RH and T values at meter levels. As the BCIM requires RH=100% for the formation of water droplets (considered to be at CLWC peak level), the RH values above the lifting condensation level (LCL) were considered as 100% disregarding the radiosonde data above the LCL (see section 2.4.2 and SI-8b).~~

(a)~~3.2.2.2~~ Mean ~~V~~vertical profiles of vapour isotopes from TES and LMDZ data

To obtain the vertical profiles of vapour isotopes, we first tried out ~~the isotope outputs of~~ a particular ~~General Circulation Model~~General Circulation Model, ~~namely,~~ LMDZ. The output data for our sampling days over Pune was provided by Dr. Camille Risi (personal communication, 2023) using the LMDZ isotope-enabled general circulation model, ~~(GCM),~~ known as LMDZ-iso (Risi et al., 2010), which is a version of the LMDZ atmospheric model adapted to simulate the natural variations of water isotopes in precipitation and vapour. Unfortunately, when the vapour isotope values from LMDZ-iso over Pune are used as inputs of BCIM, the model values did not yield good agreement with observations (results not shown). Therefore, ~~Initially, the LMDZ-derived values were also used in BCIM as inputs, but we found that a wide difference exists between the observed and model isotopic values (results not shown). We suspected that the LMDZ model did not generate the input vapour isotope profiles accurately. Possibility of such a limitation was noted by Risi et al. (2021), who observed that for high precipitation areas, the convective or mesoscale downdrafts bring depleted vapour from above into the sub-cloud layer.~~

~~Recognizing the large discrepancies arising out of using a GCM product (LMDZ) directly for both the isotopes, we tried out nex~~int the next attempt, we took recourse to the measured δDv profiles obtained from Tropospheric Emission Spectrometer (TES) ~~observations~~ pertaining to the Pune region. ~~We should note here that~~However, the TES data were not available for 2019 ~~and the available values must be modified for adapting to 2019 monsoon period~~. We assumed that ~~To account for~~ the time discrepancy can be accounted for~~,~~ if the final

Formatted: Font: Not Bold
Formatted: Indent: First line: 1.27 cm
Formatted: Font: Not Bold
Formatted: Font: Not Bold
Formatted: Indent: First line: 1.27 cm
Formatted: Font: Font color: Auto, English (U.S.)
Formatted
Formatted: Font: Pattern: Clear, Ligatures: None
Formatted: Font: (Default) Times New Roman, 10 pt
Formatted: Font: (Default) Times New Roman, 10 pt

profiles areare ~~constrained~~ approximated by using the measured daily-scale ground-level vapour isotope ratios as a boundary ~~condition~~ constraint while maintaining the shapes of the TES δDv profiles. We should also mention here that apart from TES the vapour δD data, in principle, can be obtained from one other source, namely, Atmospheric Infrared Sounder (AIRS). However, isotope vertical profiles obtained from AIRS and used in the BCIM ~~runs~~ (after suitable boundary ~~modifications~~constraints) produced ~~rain isotopes~~model rain values that were widely different from the observed values. The possible causes for this are explored in Supplementary Information SI-7 and Fig. S7-1.

~~See Supplementary Information SI-7 and Fig. S7-1.~~

The derivation of vapour isotope profiles ~~applicable for our sampling days in 2019 requires an adjustment, which would allow merging of lower level data with the TES observations at upper layers. This assumes~~ is based on the assumption that the shapes of the TES average profiles were applicable as far as the vertical variation is concerned. The TES satellite provides δD_v values of moisture at 17 pressure levels with a 5.3 km × 8.4 km footprint during the years 2005-2009 over a box covering the study region (16°-20° N; 72°-76° E). Using these data sets, we can derive an average TES profile and assume it to be representative of the shape of the mean monsoon (June ~~September) profile~~September) profile. Our station at Pune falls within this box, but there is an inherent assumption that the average over a ~45 km^2 area represents the vapour over a small sampling location if we force the abovementioned boundary constraint. Under this~~. The only justification is the~~To achieve closer representation of our sampling location, we use of a ~~boundary~~ constraint, ~~where~~ the TES average profile is adjusted to match the measured ground vapour value at the sampling location. A support for this assumption is provided by the back-trajectory analysis that indicates that the Pune moisture source is always from the Arabian Sea (see Fig. S4-1). ~~In addition, the back trajectory analysis indicates that the moisture source is always from the Arabian Sea, where the vapour is carried inland by the streaming air mass (see Fig. S4-1).~~ Interestingly, an average of ~~17 years of data of~~ $\delta^{18}O$ values of rain waters in Bombay (from 1961 to 1978) is -1.3‰ (Bhattacharya et al., 2003), close to the Pune average value of -1.1‰ from the present study. It shows that Pune being located 150 km upstream of Bombay receives moisture of similar composition as Bombay (~~possibly added by some~~with potential addition from ~~evaporation component on the way). Therefore, our assumption of a large areal~~ spatial average representing a small location is not expected to be wrong, at least as far as the vertical variation is concerned.

(b) ~~3.2.2.3~~ ~~Daily scale profile by~~~~The~~ adjustment technique ~~to derive the vapour isotope profiles~~

As mentioned, ~~T~~the δD and d-excess profiles for each date from the TES data were obtained by adjustment with the measured surface values. We analysed the available TES δD profiles ~~(digital values)~~ for the years 2005-2007 and adopted three profiles from the data sets which correspond to the ~~Minimum~~minimum, ~~Mean~~ mean and ~~Maximum~~ maximum surface vapour δD values ~~observed in the present study at the surface level~~. Each of these three profiles was fitted with polynomials and the coefficients of these polynomials were treated as functions of the surface values. Once we get these functions, we can obtain the vapour isotope profiles for any day by using that day's surface value. This exercise was necessary to translate the variation of the discrete TES values into an analytical form, allowing for the easy calculation of vapour isotope values at each height (at one meter resolution) from the drop introduction point to the ground level, resulting in a smooth shaped profile.

~~This exercise was necessary to translate the digital TES values into an analytical form, allowing for the easy calculation of vapour isotope values at each height (at one meter resolution required for the BCIM inputs) from the uppermost drop introduction point to the ground level, resulting in a smooth shaped profile.~~

A similar exercise was conducted to obtain the daily d-excess profile from the LMDZ ~~GCM~~ output ~~for Pune in 2019~~ and normalising the profile to the measured vapour d-excess value. In brief, this was done by using the available δD and $\delta^{18}O$ profiles from LMDZ output for three cases (Mean, Max and Min surface values), fitting 4th-order polynomials: $Ah^4+Bh^3+Ch^2+ Dh + E$, and then constructing the d-excess profiles for three cases with five coefficients. Five coefficients were used to get higher precision in fitting. Again, fitting was done for each of the polynomial coefficients (A, B, C, D and E) as a function of surface value. ~~and then used them to get the dex profile for each day~~Using the coefficients, d-excess profiles are obtained for each day. This procedure is discussed in detail in SI-8a. Fig S8b-1 and Fig S8b-2 ~~in the Supplementary Information SI-8b~~ show the input profiles (RH and T), and (δDv and d-excess) respectively, for the three runs~~,~~: Run-1, Run-2 and Run-3.

~~The above exercise means that by using the observed ground vapour value as a boundary value, we obtain the desired profiles for δD and dex for each day from an analytical fitting of digital isotope data from TES (adopted) and LMDZ. We used a multi order polynomial to get the fitting as accurately as possible, especially for d-excess. Obviously, this~~The method of estimating the vapour profile, constrained by surface vapour measurements, assumes that the vapour aloft is related to the surface value. This assumption may not be strictly correct~~.~~, ~~But~~ but it allows us to check if the BCIM, under the surface constraints, yields better rain isotope ratios ~~at the ground~~ compared to the Rayleigh model while being consistent with the TES measurements of vapour aloft.

~~**3.2.2.4 Run-2 results**~~

The above profiles were employed in BCIM to generate the daily-scale $\delta^{18}O$, δD and d-excess values of surface rains (Fig. 5e-5h). However, the results do not show much improvement compared to the Run-1 (Fig. 5e-5g) despite showing a larger variability in the Δδ–Δd plot (Fig. 5h); the Δδ values varied from -4.7 ‰ to 11 ‰ and Δd from -1.8 ‰ to -12.4 ‰. As in Run-1, all the model data points fell in the 3rd quadrant of the Δδ–Δd cross plot (Fig. 5h and Fig. 5d). In conclusion, ~~B~~both Run-1 and Run-2 simulations fail to yield a good match between the observed and model values (especially the d-excess). The rain δD values differ by about -8 ‰ to 20‰. The model d-excess values are higher (by 0 to 15‰). Interestingly, the model rain values of Run-1 and Run-2 are quite close (within ±2.5‰) despite RH and T and isotope profiles being very different. This suggests that the assumption of surface vapour value as the boundary constraint, as used in both these runs, is the main determinant for rain isotopes.

3.2.3 Possible sources of failures in predictions of Run-1 and Run-2 ~~: Tuning of Vapour Isotope Profile~~

The ~~mismatch in the case of~~failure of Run-1 and Run-2 predictions, ~~,~~ as discussed above, indicates that we still need to modify the input profiles to obtain a ~~better~~ good match with the observed values. ~~Below, we discuss how we go about this task.~~

Formatted: Indent: First line: 0 cm

~~**3.2.3.1 Possible sources of discrepancy in Run-1 and Run-2**~~

~~Based on the previous discussions, we~~ ~~We note~~It is easy to see that the ambient vapour isotope values have the maximum impact on the model rain isotope values. This can be shown quantitatively by a multiple regression analysis of rain isotope values with four influencing factors (RH, Temperature, surface δDv and drop diameter) in their normalised forms. The normalised values (the ratio of anomalies of the daily data and 1σ standard deviation) of the model rain isotope ratios $\delta D_{mod\text{-}rain}$ obtained from Run-2 for the 29 sampling days were regressed with the normalized values of these four variables. We obtain the following multiple regression equation (normalized):

$$\delta D_{mod\text{-}rain} = -0.114*RH+0.035*Temperature-0.059*diameter+0.986*\delta D_v \quad (1)$$

This equation indicates that the major influence on the model rain isotope value is from the ambient vapour δDv (with a coefficient of nearly one, meaning +1‰~~%~~ change in δDv would result in +1‰~~%~~ change in the rain δDv). In contrast, the influence of RH, for example, is only one-tenth ~~(~~ in opposite direction~~) for the same percentage change~~. The influences of temperature and droplet size are still less. It is logical to assume that the main source of discrepancy in ~~Run-1 and~~ Run 2 simulations is improper vapour isotope profiles and therefore, for tuning, a change in the vapour isotope value would be the most effective.

It seems that the true profile for a given date does not coincide with the adopted one based on extrapolating to the measured surface value, as assumed by the boundary constraint. In other words, the vapour aloft may not be derived entirely from the surface vapour as measured at our sampling location. ~~One possible explanation~~The reason for this could be a significant contribution from the ~~small-scale~~ local surface moisture having a different isotopic composition (evaporation or evapotranspiration from water bodies or trees within a few hundred meters). However, this possibility can be ruled out as a study using satellite data showed that due to high humidity during the monsoon season evaporation/ evapotranspiration (~0.5 mm day^{-1}) adds a negligible amount of moisture compared to the advective flux in this region (Pathak et al., 2014). However, the measured surface vapour refers to post-rain ground level vapour which may suffer from downdrafted vapour with contribution from drop evaporation. This contribution may change the surface vapour when we measure it making it different from the vapour that gave rise to the rain drops aloft.~~The search for a true profile in our case is limited by the absence of high-altitude vapour observation of δD and δ^{18}O values from an independent source or model on a daily scale.~~

3.2.4 Run 3 results

~~**3.2.3.2 Modification of the isotope ratios and Run-3 results**~~

Guided by the regression equations, we tuned the vapour δD and dex input profiles (Run-3) to achieve a ~~reasonable~~ better agreement in the rain isotope values for each date (Fig. 5i-5k). The surface δD values were changed by +13.9 to -17.8‰ and the d-excess values from +3.2 to -17.1‰ while keeping the shape for daily profiles similar to Run-2 ~~(following the adjustment procedure discussed above)~~. Corresponding changes in the vapour δ^{18}O was~~is~~ from +2.9 to -1.9‰. Most of the changes were small; in the δDv, 23 out of 29 changes were within ±4% ~~(discarding six large changes)~~ and in the d-excess$_v$ 23 out of 29 changes were within ±3.4‰ ~~(discarding six large changes)~~. As a consequence of this tuning, the average d-excess of the surface vapour

Formatted: Indent: First line: 0 cm

decreased to 10.7 ‰ from the average measured value of 17.3 ‰. The resultant vapour isotope profiles of Run-3 are shown along with those of Run-1 and Run-2 in Fig. SI-8b-2. This tuning resulted in good agreement of the model values with the observed values, as designed.~~These changes improved the results considerably. As a consequence of this tuning, the average d-excess of the surface vapour decreased to ~10.7 ‰ from the measured average surface value of 17.3 ‰. To see these modifications clearly, the Run-3 vapour isotope profiles are shown along with those of Run-2 profiles in Fig. SI-8b-2.~~

A two-tailed Student's t-test shows that the Run-3 model values are close to the observed ones for all three parameters ($\delta^{18}O$, δD, and d-excess) at p=0.05 significance level (see SI-9; Table S9). The average (observation-model) d-excess difference decreases from 2.1 to 0.4. Additionally, there is close match in the $\Delta\delta$-Δd cross plot (see Fig. 5l).

~~To check the agreement, a two-tailed Student's t-test was done with observed and modelled $\delta^{18}O$, δD, and d-excess values of 29 rain samples after each of the runs. This test shows that the Run-3 model values are close to the observed ones for all three parameters ($\delta^{18}O$, δD, and d-excess) at p=0.05 significance level (see SI-9; Table S9). The outputs of Run-1 and Run-2 agree with each other reasonably well (see Fig. S9-1) for all three isotopic parameters, but they do not agree well with the observed values.~~

As mentioned above, the dex value of the near surface vapour measured during or post-rainfall may have a substantial component of downdrafted vapour from the rain evaporation zone in the sub-cloud layer. Therefore, it is reasonable to assume that the vapour which formed the rain is not represented by the measured ground vapour. The downdrafted vapour should have d-excess values higher than the rain-forming vapour because rain drop evaporation generates vapour with lighter isotope ratios but higher d-excess. So, when we measure isotopes in vapour post-rainfall, we have an artifact due to variable addition of downdrafted vapour with high d-excess. The contribution cannot be estimated easily, and it is variable. The vapour isotope values during the monsoon days change from day to day and does not have a fixed value. Therefore, we cannot take any non-rainy-day value as proxy for an un-altered vapour which is responsible for the rain formation.

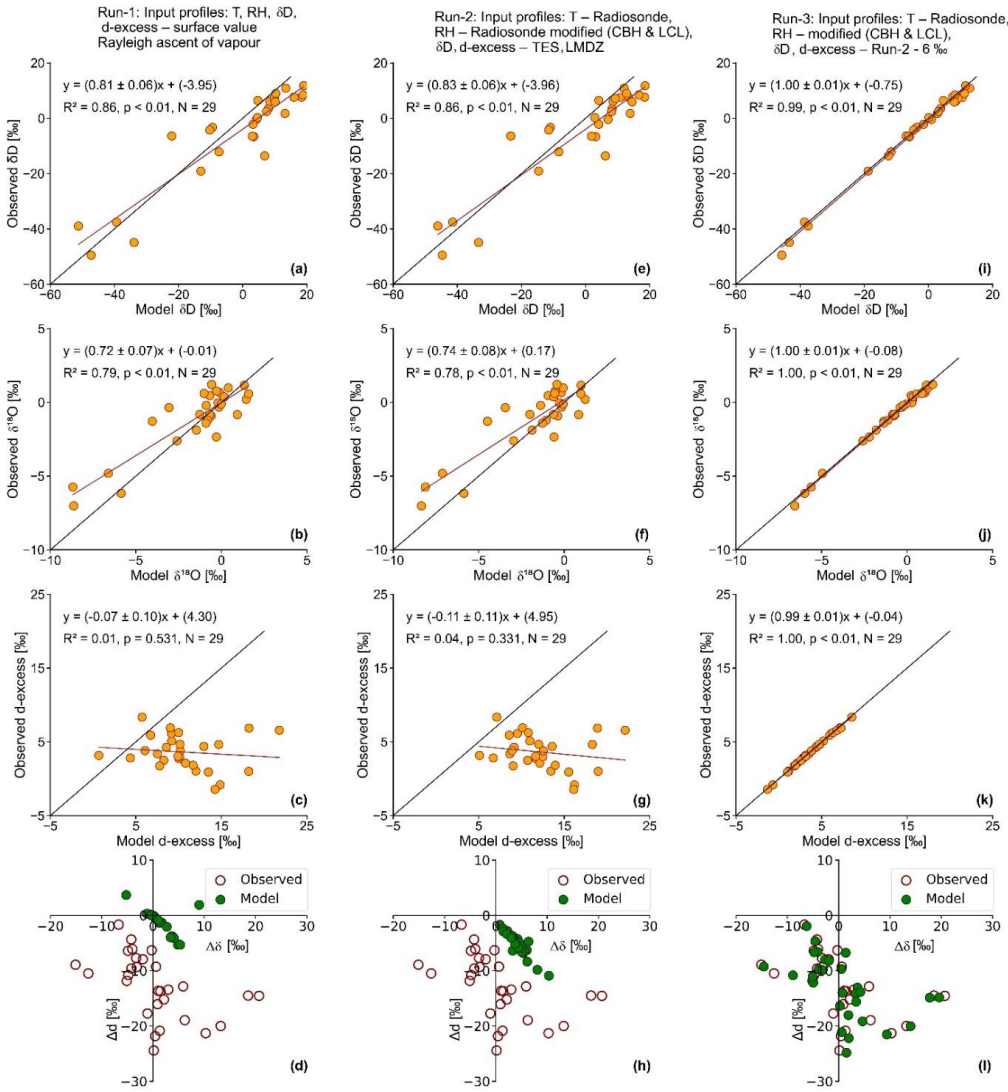

Figure 5. Scatter plots showing observed vs model values for δD, $\delta^{18}O$, and d-excess for various runs (Run-1, Run-2 and Run-3) of BCIM in the upper nine panels. The lowermost three panels show the Δδ−Δd cross-plots for the runs. The input profile sources of T, RH, vapour δD and d-excess used in the model for the three runs are given in the descriptions above. The best agreement between the observed and model values is achieved in Run-3. Run 3 uses the same RH and T as Run 2 but δD, and d-excess values are adjusted by tuning. The average d-excess reduces to ~~~10.7‰ from the observed value of ~~17.3‰ used in Run-2.

~~The physical basis behind the good agreement in Run-3 is the validity of the assumptions of the cloud microphysics of the BCIM, which calculates the evolution of the raindrops as they fall through the cloud and below cloud layers. The evolution changes the mass as well as the isotope ratio, finally culminating in the values that we measure on the ground. We think that a reasonable agreement of the isotope values is proof that the assumed cloud microphysics of the BCIM (with all assumed input parameter values) holds good for the drop~~

~~mass evolution, and therefore the drop evaporation estimated from the same model (see later) can be considered valid.~~

3.2.5~~3.3~~ Sensitivity and uncertainty of the ~~model~~ Run-3 predictions ~~in Run-3~~

~~The simulations of BCIM predict the rain isotope ratios based on assumed values of RH, T, drop size and vapour isotope ratios.~~ We did a sensitivity and uncertainty analysis of the model rain composition using Run-3~~1~~ results to study the effects of variation in vapour isotopes (δDv), ~~temperature,~~ relative humidity (RH), temperature (T)~~vapour isotopes~~, and drop size (D)~~, and the results are given in Supplementary Information SI-13~~. We find that the vapor isotope value is the most important factor controlling rain isotope ratios in the BCIM. The uncertainty of the model predicted δD and d-excess of rain are 3.0‰ and 1.7‰ respectively. In case of sensitivity, for a +10% change over the reference values of the parameters, δDv, RH, T and D, the changes in the rain δD values (in ‰) are: +7.6, -4.1, +2.6 and -0.4 respectively. BCIM Run-3 sensitivity analysis and uncertainty calculations are available in SI-13,14.

~~. Fig. S13-1 shows that the vapour isotope value is the most important factor in controlling the model rain isotope ratios. For +10% change over the reference value of the parameters, the changes in the rain δD values (in ‰) are: +7.6 (for δDv), -4.1 (for RH), +2.6 (for T) and -0.4 (for diameter).~~

~~We also determined the uncertainty of the model predictions of dD (rain) and d-excess (rain). Using the Run-3 model output values, we obtained a multi-parameter regression equation for δD (rain) as a function of the four variables (vapour isotope, relative humidity, temperature, and drop diameter) δDv, RH, T and D. With given inputs of errors in δDv, RH, T and D, the uncertainty in the rain isotope value δD_{rain} is 3.5 ‰. Using a similar exercise for the d-excess$_{rain}$ we obtain uncertainty for the d-excess$_{rain}$ as 2 ‰. The details of the calculations are given in SI-14.~~

4. Discussions

For clarity, this section is divided into two major parts (1) the discussion of the observed rain and vapour isotope ratios and what they mean and (2) the message that we get by comparing the results of the BCIM with observations.

4.1 Influence of local meteorological parameters on observed isotope ratios~~s~~

~~Water isotopes in the tropics often vary with rainfall, humidity, and temperature (Dansgaard, 2012; Lee and Fung, 2008).~~ In our data, the vapor d-excess is not significantly correlated with rainfall amount, relative humidity, specific humidity and temperature (details are provided in S10-1). ~~Scatter plots between the vapour d-excess values and local meteorological parameters such as rainfall amount, relative humidity, specific humidity and temperature are shown in Fig. S10-1. The d-excess of vapour shows only a marginal positive correlation with temperature (R^2=0.16; p-value=0.03; not significant) and a small negative correlation with relative humidity (R^2=0.22; p-value=0.01; marginally significant).~~ However, we do see synchronous low OLR values and low isotope values (in both vapour and rain) as the convective cloud bands traverse to the sampling location in Pune from southwest (Fig. 2).

Formatted: Font: Symbol

Formatted: Indent: First line: 0 cm

Formatted: Don't adjust space between Latin and Asian text, Don't adjust space between Asian text and numbers

Formatted: Left, Indent: First line: 0 cm

Rain isotopes often vary with rainfall, humidity, and temperature (Dansgaard, 2012; Lee and Fung, 2008). But the rain isotopes in Pune do not have a simple relation with the local rainfall (Fig. 2). The absence of simple isotope-rainfall correlation in tropics has also been found in several other regions (Chakraborty et al., 2016; Moerman et al., 2013; Vimeux et al., 2011). Even though a straightforward relation with local rainfall is absent, a correlation is often found with the regional convective activities (Kurita, 2013; Lekshmy et al., 2018). Risi et al. (2023) have noted that in the tropics, most of the precipitation falls under deep convective systems (see Section 3.1 and Fig. 2), which are controlled by various microphysical processes (like rain evaporation, diffusive liquid-vapour exchanges) connected through mesoscale circulations. These processes probably add on to the effect of surface meteorological parameters in this region to offset a simple dependence of rain isotopes on rainfall. However, as noted above, movement of large-scale convective bands reflected by low OLR registers its signature in both low isotope events and high rainfall (Fig. 2).

~~It is known that temperature and relative humidity of air have opposite controls on raindrop evaporation (Lee and Fung, 2008; Stewart, 1975). If the drop in evaporation~~raindrop evaporation ~~affects the rainfall amount significantly, we should have seen some relation between the rainwater isotopes and rainfall. The absence of correlation in tropics is also found in several other studies (Chakraborty et al., 2016; Moerman et al., 2013; Vimeux et al., 2011). Even though a relation with rainfall is absent, a correlation is often found with the regional convective activities (Kurita, 2013; Lekshmy et al., 2018). Risi et al. (2023) have noted that in the tropics, most of the precipitation falls under deep convective systems (see Section 3.1 and Fig. 2), which are controlled by various microphysical processes (like rain evaporation, diffusive liquid-vapour exchanges, and mesoscale downdrafts) connected through mesoscale circulations. These processes probably override the effect of surface meteorological parameters in our region.~~

4.2 Rain-vapour isotope exchange and rain evaporation

~~An~~ The observed increasing trend (13 ‰ to 30 ‰) in the vapour d-excess values associated with a decrease in the $\delta^{18}O$ values with the progress of the monsoon (Fig. 2b) is an intriguing feature and could be ascribed to significant ~~recycling of the moisture with~~ contribution from some evaporative sources. Changes in moisture sources can also cause concomitant change in isotope values in rain and vapour (Deshpande et al., 2010; Midhun et al., 2018). We investigated this possibility by forty-eight hours of air-parcel back trajectory analysis (Fig. S4-1), which shows that moisture was derived mainly from the Arabian Sea all through the season.

~~Risi et al. (2023) have discussed the possibility of down-drafted vapours as the source of such anomalously low isotope ratios in the case of Sahelian squall lines. Earlier studies over some Indian sites have shown that changes in moisture sources are often associated with a concomitant change in isotope values in rain and vapour (Deshpande et al., 2010; Midhun et al., 2018). We investigated the possibility of this by forty-eight hours of air-parcel back trajectory analysis (Fig. S4-1), which shows that moisture was derived mainly from the Arabian Sea. However, this does not rule out the possibility of minor evaporative contributions from continental moisture sources enroute or down-drafted moisture characterised by low isotope ratios and high d-excess values (Risi et al., 2010).~~

The ~~microphysical~~ process of evaporative exchange during the fall of raindrops causes isotopic enrichment in the rain which~~. Though important, raindrop evaporation~~ cannot be easily quantified. ~~As discussed~~

Formatted: Not Highlight
Formatted: Not Highlight
Formatted: Not Highlight
Formatted: Not Highlight
Formatted: Not Highlight
Formatted: Not Highlight
Formatted: Not Highlight
Formatted: Not Highlight

~~before, e~~ Evaporation is reflected in higher δ-values and lower d-excess values ~~(mean ~2 ‰)~~ of the rain samples. Froehlich et al. (2008) used d-excess values of precipitation in the Alpine region to derive the extent of evaporation using assumed end-member values of the regional vapours.

~~————~~Any isotope exchange between the rain and ambient vapour would result in correlated changes. A strong correlation between rain and vapour $\delta^{18}O$ values is indeed found (Fig. 6a; R^2=0.7, $p < 0.01$, n=29)~~, suggesting a connection between them~~. Sinha and Chakraborty (2020) also found significant positive relations (R^2>0.8) between rain and vapour $\delta^{18}O$ values over the Andaman Island. However, they did not find any anti-correlation between rain $\delta^{18}O$ and rain d-excess, as found here (Fig. 4b). The current study exhibits an ~~reasonable~~ anti-correlation between the differences in d-excess (Δd-excess$_{r\text{-}v}$) and $\delta^{18}O$ ($\Delta\delta^{18}O_{r\text{-}v}$) of rain and vapour (the subscript r-v indicates ~~Rain~~ rain isotope minus ~~Vapour~~ vapour isotope) (Fig. 6b). ~~This would be expected if evaporation of rain contributes a significant amount of vapour because the generated vapour is lower in $\delta^{18}O$ but higher in~~

~~d-excess compared to the rain.~~

As raindrops evaporate, part of the newly formed vapour may get down-drafted to lower levels~~;, and therefore,~~ the ~~two~~ rain and vapour phases at the ground level would exhibit opposite changes because the generated vapour is lower in $\delta^{18}O$ but higher in d-excess compared to the rain. This happens when the evaporative contribution is large. However, in ~~the~~ case of tropical precipitation, the fractional addition from rain evaporation is small because the ambient vapour is a large reservoir.~~we do not expect a substantial contribution from rain evaporation to the ambient vapour because the latter is a large reservoir.~~ It has been shown in several earlier studies that the total rain ~~is derived from~~constitutes only a few percent of the overhead vapour mass (Pathak et al., 2014; Rahul et al., 2016). Earlier studies have also shown that vapour d-excess values do not exhibit any systematic change in central or southern WG stations, ~~although~~but~~, surprisingly,~~ their rain $\delta^{18}O$ values exhibit slight but gradual depletion (1 ‰ to -10 ‰) in the latter part of the monsoon (Lekshmy et al., 2018; Rahul et al., 2016). The negative correlation found in this study, albeit minor, suggests that the ground-level vapour gets a significant contribution from drop evaporation. How can moisture generated by drop evaporation ~~over the falling path~~ during rain drop descent contribute to the ground-level vapour? This is possible when there is a strong downdraft associated with intense monsoon rains (Risi et al., 2023). In a modelling study, Mandke et al. (1999) pointed out that deep convective cloud systems contain both upward and downward components. The downward motion is driven by the evaporation of falling precipitation and the dragging of the ambient air and vapour by big droplets. This downdraft brings moisture down from above and increases the vapour d-excess at the surface (Risi et al., 2010; Kurita, 2013; Aemisegger et al., 2015).

The existence of drop evaporation is further supported by a relation between Δd-excess$_{r\text{-}v}$ and surface relative humidity (RH; R^2=0.31; Fig. 6c). The difference between rain and vapour isotopes is ~~more~~ higher (more negative) in lower RH and less in higher RH~~, as expected~~ (Stewart, 1975). A similar analysis (Xing et al., 2020) in China also found that the change in isotopic composition is large when RH is less than 60 %.

Formatted: Indent: First line: 1.27 cm

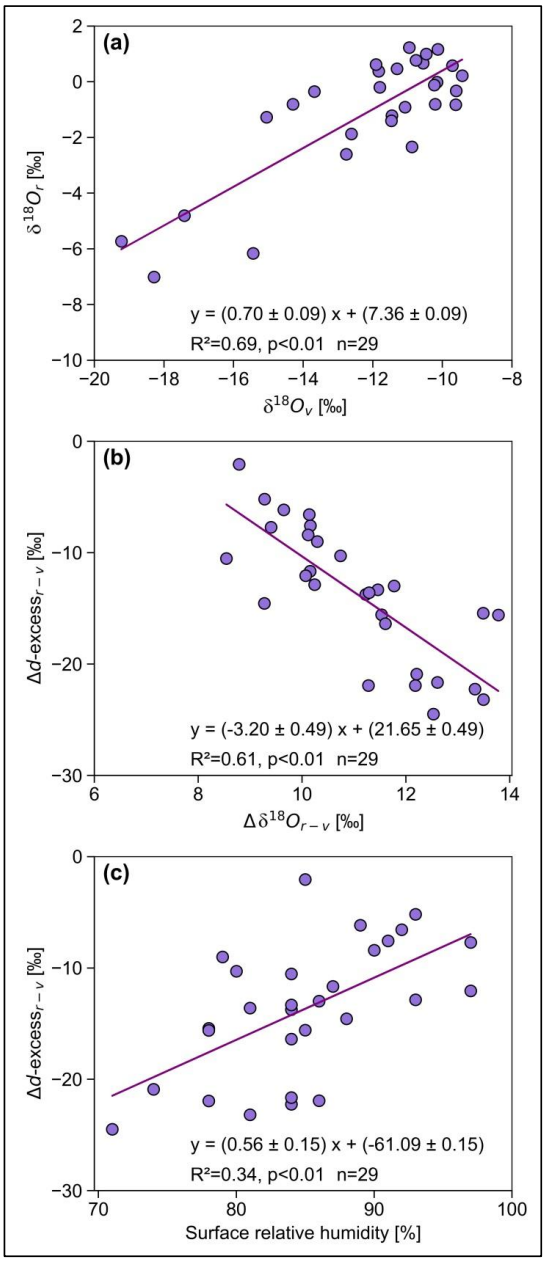

Figure 6. The correlations between **(a)** $\delta^{18}O$ of rain ($\delta^{18}O_r$) and $\delta^{18}O$ of vapour ($\delta^{18}O_v$) at the ground level; **(b)** the difference in d-excess of rain and vapour (Δd-excess$_{r\text{-}v}$) and $\delta^{18}O$ ($\Delta\delta^{18}O_{r\text{-}v}$) showing that the rain value is lower in d-excess whereas it is higher in $\delta^{18}O$; **(c)** difference in the d-excess of rain and vapour (Δd-excess$_{r\text{-}v}$) and ground level relative humidity (RH).

Falling raindrops and the ~~water~~ vapour in the atmospheric column constitute an interacting two-phase system,~~ especially below the cloud base. On the way down~~Below the cloud base, the water molecules are constantly exchanged between these two phases depending on the ambient RH and temperature. ~~This makes the~~

~~system evolve towards an isotopic steady state.~~ The difference between isotopes (δD and d-excess) of vapour in equilibrium with raindrops and the observed surface vapour (~~defined as~~ Δδ and Δd~~,~~ respectively) is a useful ~~to quantify the~~signature of departure from equilibrium exchange. Graf et al. (2019) demonstrated ~~the importance of~~how the ~~a~~ Δδ-Δd plot ~~to~~ represents the effect of sub-cloud processes, such as evaporation and equilibration, which influence the ~~water~~ rain isotopes. The time series of Δδ values (Fig. 7a) for the Pune ~~precipitation~~ rain samples shows that the values varied between -15 ‰ and 21 ‰. For Δd, the time series shows negative values in all cases (ranging from -2 to -24 ‰). The close-to-equilibrium samples correspond mostly to the high-humidity period in July (Fig. 7b). Fifteen samples ~~indicate~~ show the influence of below-cloud evaporation with positive Δδ values and associated ~~with~~ strongly negative Δd values (up to -20 ‰).

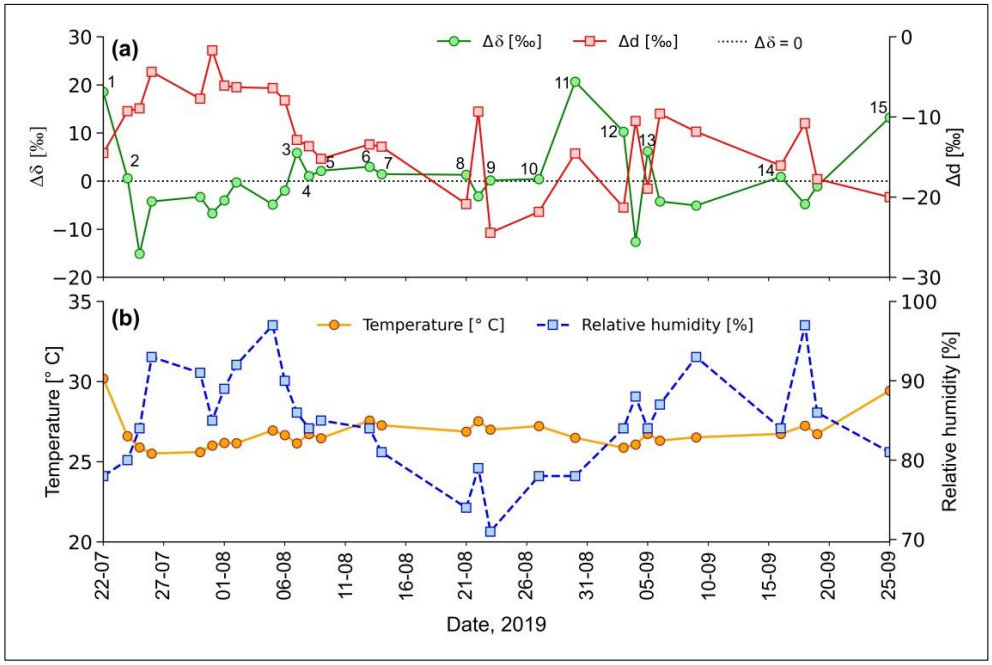

Figure 7. (a) Time series of Δδ and Δd of the rain samples collected during 2019 monsoon (July to September) in Pune. Δδ and Δd values (total points=29) denote rain-equilibrated vapour isotope minus the surface vapour isotope. The blue dotted line indicates Δδ=0. All data points where Δδ>0 are marked with numbers ~~totalling~~totaling 15, **(b)** Time series of daily average surface temperature and relative humidity recorded at IMD observatory at Pune.

A Δδ-Δd scatter plot ~~based on these observed data~~ (Fig. 8) shows that none of the rain samples is in equilibrium with the corresponding ground-level vapour. If the equilibrium pertained, the corresponding point~~s~~ would plot at the origin. ~~15~~ Fifteen ~~sample~~ points fall in the lower right quadrant of the diagram (positive Δδ and negative Δd values), where the raindrop evaporation is relatively more significant~~, as per Graf et al. (2019)~~. ~~We note that t~~The ~~observed~~ rainfall amount for these samples was low (less than 5 mm) ~~for these samples~~, ~~which is~~ consistent with a substantial evaporation effect. ~~14~~ Fourteen samples have both negative Δδ and Δd values (located in the 4th quadrant), indicating incomplete equilibration with near-surface vapour. The crucial driving factors for below-cloud processes seem to be the size of raindrops ~~and~~ related to the intensity of precipitation. This is ~~primarily~~ because raindrops with larger diameters correspond to increased intensity and have shorter residence times in the atmospheric column. As a result, they experience reduced evaporation ~~while descending toward the ground~~during descent. ~~However,~~It is to be noted that the drop size in this study was not measured by disdrometer directly. They were estimated from rain rate using Marshall-Palmer relationship.

Formatted: Superscript

Formatted: Font: 10 pt

Formatted: Font: 10 pt

Formatted: Font:

~~the drop size in this study was not derived by an independent method~~disdrometer method ~~independently of rain rate. They were based on rain rates or precipitation intensity through M-P relation and are not independent. The rain rate and droplet diameter are directly related through the M-P relationship used here, so~~Therefore, ~~-~~larger rain rates will always translate to larger droplet size. This physical relationship is thought to be a result of increased collision-coalescence during higher rainfall intensity (Law et al., 2021).

~~A clearer demonstration of the relation between rain rate and drop size was provided by Law et al. (2021), who showed that higher rainfall intensities are characterised by closer distances among raindrop particles. This results in higher chances for smaller raindrops to collide and to coalesce into larger droplets before falling from the cloud. We note that our data is consistent with their conclusion.~~

Distribution of points in the Δδ-Δd plot (Fig.8) shows that 10 samples with <5mm/day rain rate fall in the lower right quadrant compared to 5 in the left quadrant. This suggests that drop evaporation is a dominant process in low rainfall events (where smaller drop sizes dominate). In Fig.8, the size of the points denote drop size, and the colour of the points denote rainfall. ~~To see the rainfall or drop size effect more clearly the size of the points was characterised in terms of drop size, and the colour of the points was varied, indicative of rainfall (Fig. 8).~~ It seems that larger drop size points with higher rainfall ~~are always~~plot in the lower left quadrant. This indicates ~~that in such cases~~that for larger sizes~~,~~ the memory of the isotopes is partly retained even after the sub-cloud evaporation~~ due to larger sizes~~. ~~The 29 sampling~~Twentynine ~~points~~samples are nearly equally distributed in the two quadrants, suggesting an equal number of equilibration-dominant and evaporation-dominant rain events. It is to be noted that deep convective rains during the monsoon exhibit significantly higher mass-weighted diameter compared to shallow convective rains or stratiform rains (Kumar et al., 2025). The five big diameter points in the lower left quadrant correspond to ~~such~~ cases of deep convection.

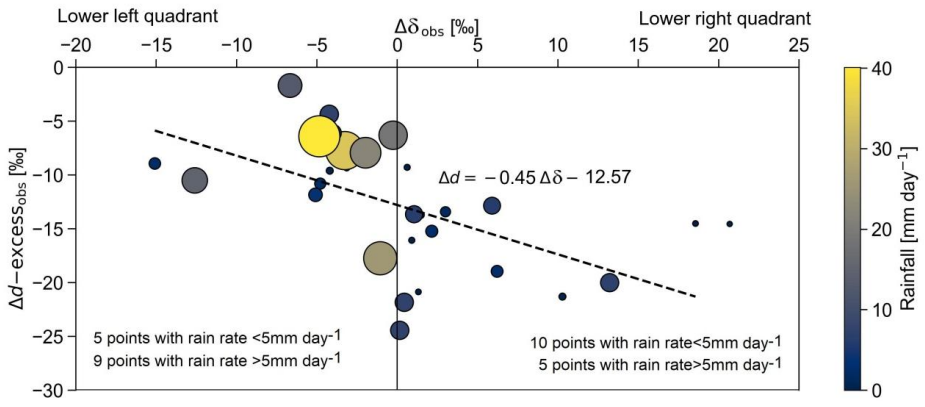

Figure 8. The Δδ-Δd plot based on observed values for various rain rates. The size of the sample circles indicates drop size; their variation is also associated with the rain rate (scale on right). We note that most of the 4th quadrant (lower left) points are of bigger size and those in the 3rd quadrant (lower right) are of small size. The line shows a good fit to the data with a slope of -0.45.

Formatted: Font: 10 pt

Formatted: Indent: First line: 1.27 cm, Space Before: 0 pt

The regression line in the Δδ-Δd cross plot (Fig. 8) ~~based on all 29 observed values~~ has a slope of -0.45 based on Bootstrap analysis (See SI-11). ~~This is more than the slope of -0.30 reported by~~ In contrast, Graf et al. (2019) obtained a smaller value of -0.30 for their study area, Zurich, Switzerland. The difference is intriguing and merits a discussion. Their study was based on short-time intra-event samples (covering about 16 hours and each rain sample being collected for 10 to 15 min) in a mid-latitude region, whereas Pune samples were 29 daily rain collections in a tropical region (covering a few months and each collected for 24 hours). ~~29 daily samples in a tropical region (covering a few months and each rain sample being collected for 24 hours) are used in the current study.~~ A set of complex processes operates to dictate the value of the slope, and Graf et al. (2019) pointed out that the slope could represent a balance between below-cloud evaporation and equilibration. They suggested that it would be insightful to explore the slope for other climatic regions, hinting that the slope will help assess the evaporation ~~magnitude~~. A quantitative estimate of the evaporation fraction can be obtained from BCIM by using the mass loss parameter in the output ~~discussed later in~~(see section 4.3).

~~Graf et al. (2019) showed that a~~At higher humidity ~~(lower~~the evaporation is lower~~)~~, the change of Δd is ~~negligible~~smaller, and this leads~~ing~~ to a lower slope. Conversely, when the temperature is higher, the slope is higher due to higher evaporation. The slope value is ~~essentially~~ determined ~~due to~~ by a differential effect in evaporative fractionation. Evaporation decreases rain d-excess but increases rain δD but~~. However,~~ the magnitudes of these changes (negative for d-excess and positive for δD) are not the same. Fractionation values (involving equilibrium and kinetic ~~factors~~effects) show that the change in δD is larger compared to that in d-excess (about 30% of the δD change, considering the absolute values). This is because in evaporation, the kinetic ~~effect~~ fractionation (KF) operates ~~in addition to~~over and above the equilibrium fractionation, and ~~that~~ the KF has more influence on δD compared to $\delta^{18}O$. If the evaporation is higher (due to higher temperature and lower RH), the deviation from the equilibrium fractionation ~~line~~ will be more, and the slope will be higher. In the frontal systems of Switzerland, the temperature was about 12°C and RH about 80% (Graf et al., 2019) ~~compared to~~whereas in Pune the ~~, where~~ T was about 25° C and RH about 85%. ~~We see that~~Even though the RH wa~~i~~s nearly similar, ~~but~~ the temperature wa~~i~~s much higher in Pune.~~-~~ This resulted in higher slope for Pune (see next section).

~~The normalized multiple regression equation of evaporation fraction as a function of RH, T and size (diameter D), given below, shows that temperature plays an important role (nearly as much as RH for evaporation):~~

~~Normalied Evaporation Fraction (norm) = -0.329* RH +0.370* Temperature -0.665* Diameter (2)~~

~~For the larger values of Pune temperatures, we expect more evaporation, which leads to the higher slope value of -0.45 for Pune compared to -0.30 for Zurich. The multiple regression equation for evaporation shows that drop size is the major determinant for evaporation.~~

4.3 Estimate of raindrop evaporation and its uncertainty

Formatted: Indent: First line: 1.27 cm

Formatted: No widow/orphan control

The output of BCIM in Run-3 predicts that the mass of the drop reduces as it falls. The ratio of final mass to the initial mass (m/m_o) can then be used to estimate the fractional mass loss suffered by the drop on its way down. The difference ($1-m/m_o$) represents the effective rain evaporation. With this definition, a time series of evaporation values (Fig. 9a) shows variation from ~~4~~ % to 6~~10~~ %. The ~~(~~average evaporation is ~~~~ 23 %~~)~~ if we consider all 29 values. But there are four large values 45, 47, 58 and 61% all of which correspond to low rainfall or small drop size (Fig. 9d). If we exclude them the average is 18% (n=25). As expected, drop evaporation is inversely related to relative humidity (Fig. 9b) and drop diameter (Fig. 9d) but directly proportional to the temperature (Fig. 9c). The relative importance of the three determining factors, namely, RH, T and drop size is seen through the multiple regression equation of evaporation fraction. Here we should use normalized multiple regression because simple (or unnormalized) multiple regression uses variables in their original units, while normalized multiple regression transforms all features onto a similar scale, allowing for direct comparison of feature importance. The *normalized* evaporation fraction as a function of normalized values of RH, T and size (diameter D) shows that (1) drop size is the major determinant and (2) temperature plays an important role, nearly as much as RH, for evaporation.

Normalized Evaporation Fraction = -0.329* RH +0.370* Temperature -0.665* Diameter (2)

For the larger values of Pune temperatures, we expect more evaporation and this leads to the higher slope value of -0.45 (in the $\Delta\delta$-Δd cross plot) for Pune compared to -0.30 for Zurich, as noted in the previous section.

~~. As expected, drop evaporation is inversely related to the surface humidity (Fig. 9b) and drop diameter (Fig. 9d) but directly proportional to the temperature (Fig. 9c).~~

~~T~~The evaporation was particularly high (6~~10~~ % and 59 %) on 22 July and 21 August ~~when humidity was relatively~~due to combined effect of low RH (78 % and 74 %), and ~~the temperature~~ high temperature (30 °~~-~~C and 27 °~~–~~C) and ~~the~~ small diameter ~~small; the combined effect resulted in high evaporation~~ (Fig. 9a). On average, ~~T~~the ~~deduced~~ evaporation fractions are moderately high (23±16) % ~~which is~~ consistent with the observed anti-correlation between d-excess and $\delta^{18}O$ of rain samples (Fig. 4b).

Formatted: Indent: First line: 0 cm

Formatted: Font: Symbol

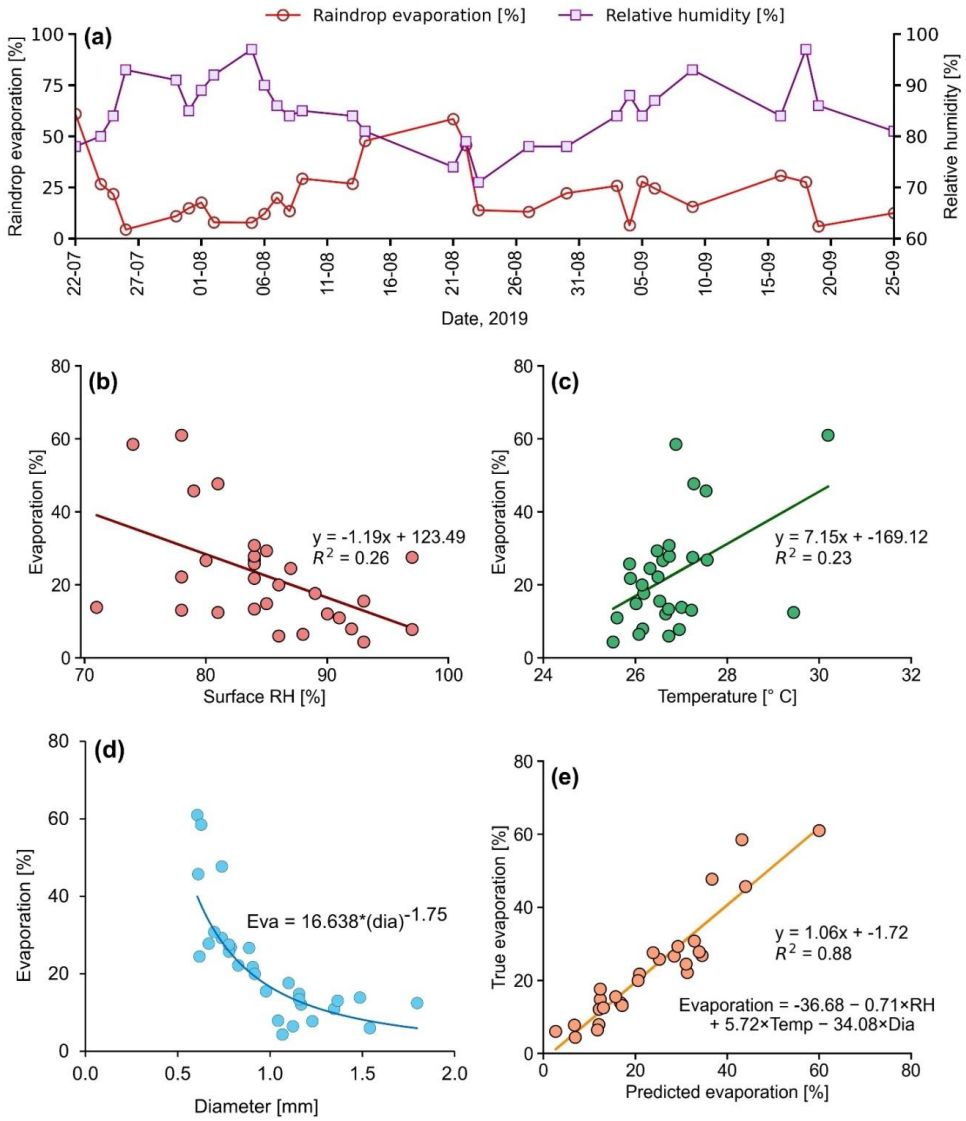

Figure 9. (a) Time series of raindrop evaporation using BCIM simulation (Run-3) and surface relative humidity. The regression between raindrop evaporation fraction with **(b)** RH, **(c)** temperature, and **(d)** drop diameter. **(e)** Multiple regression analysis yields the equation shown in the inset. The regression equation prediction of evaporation explains nearly 88% of the variance.

4.4. Uncertainties in δD_r and d-excess$_r$ using Run-3 outputs

Using the Run-3 model output values, we obtained a multi-parameter regression equation for δD (rain) as a function of the four variables (vapour isotope, relative humidity, temperature and drop diameter) δDv, RH, T and D as below:

$$\delta Dr = 87.88 + 1.137 * \delta Dv - 0.257 * RH + 1.052 * T - 3.785 * D \quad (1)$$

A similar multiple regression for d-excess rain yields the equation.

$$\text{d-exr} = -10.5557 + 0.60164 * \text{dexv} + 0.169599 * RH - 0.31632 * T + 2.2921 * D \quad (2)$$

Using the standard quadratic formula for error (Farrance and Frenkel, 2012), when the dependent variable δDr is a function of δDv, RH, T and diameter D, the error σ(δDr) is given by:

$$\sigma(\delta Dr)^2 = (\partial \delta Dr/\partial \delta Dv)^2 * \sigma(\delta Dv)^2 + (\partial \delta Dr/\partial RH)^2 * \sigma(RH)^2 + (\partial \delta Dr/\partial T)^2 * \sigma(T)^2 + (\partial \delta Dr/\partial D)^2 * \sigma(dia)^2 \quad (3)$$

Where σ denotes the uncertainties in δDv, RH, T and D, and the quantities in brackets express the partial derivative of δDr with respect to the variable. The regression coefficients were used as the partial derivatives. The vapour isotope δDv has an error of 2‰. The absolute uncertainties associated with RH and T in Radiosonde observations are 8% and 0.3° C (Sapucci et al., 2005) but they vary from day to day. The absolute difference is taken as the daily scale uncertainty. The error for each day is then taken as the absolute difference divided by √2 (to get standard error of the mean of two observations).

To obtain drop size error, we note that the mean and standard deviation of the diameter of drops (as calculated from the Marshall-Palmer relation using the rain rates) considering 29 samples are 1.00 mm and 0.3 mm i.e., the standard deviation is about 30% of the mean diameter. However, Tokay et al (2001) quote an uncertainty estimate for the size, derived based on Marshall-Palmer ~~M-P~~ distribution, which is less, about 20% and which we adopt. Pune drop diameter varies from 0.606 to 1.796 mm over the 29 days. Taking the error in each day's diameter as 20% of that day's value, the individual error varies from 0.12 mm to 0.36 mm.

With these inputs, the uncertainty in the rain isotope value δD_{rain} is 3.5 ‰. Using a similar exercise for the d-excess$_{rain}$ we obtain uncertainty for the d-excess$_{rain}$ as 1.7 ‰.

4.5 The uncertainty in the evaporation fraction

Among the controlling factors for evaporation, the temperature does not vary much (26.8±1.0 °C) or about 4%, while for RH, the variation is slightly larger (85±6 %) or 7%. The diameter variation, on the contrary, is much higher, ~~at~~ about 30% (1.0±0.3 mm) and has a higher impact on the evaporation. The net uncertainty in the evaporation fraction due to combined uncertainties in RH, T and dops size can be determined by a simple multiple regression equation (using unnormalized variables) as given below. The Evaporation Fraction (EF) was regressed with RH (in %), Temp (in °C) and the drop size D (diameter in mm). and yields:

$$\text{Evap. Fraction} = -36.68 - 0.71 * RH + 5.72 * T - 34.08 * D \quad (4)$$

~~Evaporation Fraction = -36.68-0.71*RH+5.72*T-34.08*D (3)~~

The equation (3a) can be used to estimate the error in drop evaporation, knowing the uncertainties in RH, T and D and using the partial regression coefficients as partial derivatives. Using the standard quadratic formula for error we write:

~~Using the standard quadratic formula for error (Farrance and Frenkel, 2012) we obtain:~~

$$\sigma(EF)^2 = (\partial EF/\partial RH)^2 * \sigma(RH)^2 + (\partial EF/\partial T)^2 * \sigma(T)^2 + (\partial EF/\partial D)^2 * \sigma(D)^2 \quad (5)$$

Where σ denotes the uncertainties in EF, RH, T and D, and the quantities in brackets express the partial derivative of EF with respect to the variable. The uncertainties associated with RH, T and drop size have been discussed above (section 4.4). Adding these three errors by the above quadratic formula, we obtain the error in the evaporation fraction for 29 days which vary from 7.4 to 13.8 % (for EF values from about 5 to 61%). The average for 29 days is ±8.9% which is taken as overall error in the evaporation estimate.

~~Where σ denotes the uncertainties in EF, RH, T and D, and the quantities in brackets express the partial derivative of EF with respect to the variable. The uncertainties associated with RH and T in Radiosonde observations are 8% and 0.3° C (Sapucci et al., 2005), and the uncertainty of the diameter is 20%. Using the above equation, the error σ(EF) varies from 7.4 to 13.8 % (for EF values from about 5 to 61%). The mean error is ±10%.~~

4.6 Evaporation and rainfall relation

Evaporation fraction plotted as a function of rainfall (Fig. 10) shows a power law. For smaller rainfall range (less than 5 mm day^{-1}), evaporation affects the rainfall significantly. The reason is that smaller rainfall is usually associated with smaller drops, which are very sensitive to evaporation, resulting in a power law. If the EF increases by 10% (say from 15 to 25%) the rainfall reduces by about 4 mm/day (from 5 to 1 mm/day).

~~Evaporation fraction plotted as a function of rainfall (Fig. 10) shows that the two parameters are related by a power law. For a smaller rainfall range (less than 5 mm day^{-1} to 10 mm day^{-1}), the evaporation affects the rainfall significantly. The reason is that smaller rainfall is usually associated with smaller drops, which are very sensitive to evaporation, resulting in a power law.~~

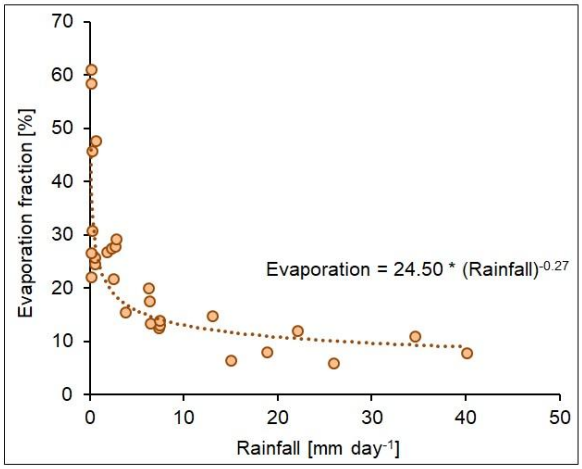

Figure 10. Scatter plot shows relationship between the estimated drop evaporation and rainfall in Pune. The black dashed line indicates the best-fit power law. Higher rainfall implies drops of bigger size and hence lower evaporation fraction.

It is instructive to compare our results to the evaporation estimates obtained in similar studies carried out in other climatic regimes. Using a steady state one-dimensional model of rain in the North Atlantic Trade

Wind region (Barbados), Sarkar et al. (2023) found a high value of 63% (63±23 %) for raindrop evaporation (using radar reflectivity data on rain evaporation flux), which is three times more than our average value of 23% (23±16 %). The reason for the large difference in Pune evaporation from Barbados is possibly due to a large difference in drop size and RH. A comparison reveals that in Barbados, the drop sizes were much smaller (from 0.1 to 0.6 mm) in comparison to ours (from 0.606 to 1.796 mm). The Barbados drops were so small that in some cases (smaller than 0.3 mm on 4 February 2020), they evaporated completely (evaporation ~ 100%) during descent. In addition, in their sampling region, the RH was lower, ranging from 65% to 80%, compared to ours (74% to 97%). Smaller drop size and lower RH lead to higher raindrop evaporation. In contrast, only four high evaporation days (more than 45%) occurred in Pune out of 29 sampling days. We also note that their drop sizes varied over a wider range, leading to a larger variability compared to our study.

~~It is instructive to compare our results to the evaporation estimates obtained in similar studies carried out in other climatic regimes. Sarkar et al. (2023), in a steady state one dimensional model study of rain in the North Atlantic Trade Wind region (Barbados), found a high value of 63% (63±23 %) for raindrop evaporation (using radar reflectivity data on rain evaporation flux), which is three times more than our average value of 23% (23±16 %). We have only four high evaporation days (more than 45%) out of 29 sampling days. The reason for the large difference in Pune evaporation from Barbados is possibly due to a large difference in drop size and RH. A comparison reveals that in Barbados, the drop sizes were much smaller (from 0.1 to 0.6 mm) in comparison to ours (from 0.61 to 1.80 mm). Their drops were so small in some cases (smaller than 0.3 mm on 4 February 2020), that the drops completely evaporated (evaporation ~ 100%) during the fall. In addition, in their sampling region, the RH was lower, ranging from 65% to 80%, compared to ours (74% to 97%). Smaller drop size and lower RH lead to higher raindrop evaporation. We also note that their drop sizes varied over a wider range, leading to a larger variability compared to our study.~~

In a similar study as here, rain and vapour isotopes were measured in a cold-front passage over Zurich during 19-25 July 2011, and the data were interpreted by an isotope-enabled regional weather prediction model COSMOiso (Aemisegger et al., 2015). The authors showed that by switching off the raindrop evaporation, the rainfall increased by about 75% because the cooling induced by evaporation causes diminished convective activity. The estimated average evaporation in their study was about 40%. This value is nearly twice our value. The reason is probably a smaller drop size and lower RH; ~~as stated in their paper~~The authors write: “weak rainfall intensities (small droplets and thus lower falling velocities), and possibly lower relative humidity in the air column could have contributed to the evaporative enrichment of precipitation”.

4.7 Limitations and uncertainty of the derived parameters

The isotope technique and the BCIM are associated with the following limitations:

(a) We used TES satellite data averaged over 2005-2009 to guide our choice of vapour isotope profiles, but the year of analysis was 2019. In this matter, there is no way to ascertain the degree of deviation of the true profile from the adopted ones in Run-3.

(b) There are limitations on the use of RH and T from radiosonde. The mean radiosonde data for Pune are expected to be reasonable if we can show that the difference between the two consecutive measurements is not large. Sondes are launched at 00 and 12Z and are generally not carried out when there is rain. We determined that two soundings taken on the same day are similar to within 8% RH and 1^{o}C on most days.

Formatted: Font: (Default) Times New Roman, 10 pt

Formatted: List Paragraph, Indent: Left: 0 cm, Hanging: 0.63 cm

Formatted: Indent: Left: 0 cm, Hanging: 0.63 cm, Numbered + Level: 1 + Numbering Style: a, b, c, … + Start at: 1 + Alignment: Left + Aligned at: 1.27 cm + Indent at: 1.9 cm

Analysis of sonde daily variability can be found in supplementary information. We also show through sensitivity analyses and multiple regression analyses that the effects of the daily scale variation in RH and T on model rain isotope values and evaporation fraction are not significant. We demonstrate further that the RH and T data from the radiosonde is more reliable than the same obtained from any satellite datasets. The $\delta^{18}O$ profiles were adopted based on the δD and $\delta^{18}O$ profiles obtained from the LMDZ model. Run-3 uses radiosonde for the thermodynamic profile, δD from satellite data from 2005-2009, and ^{18}O from the d-excess of the LMDZ extrapolated to the observed vapour measurement at the ground. We realize that there are major concerns with these inputs coming from different data products that all have different spatial/temporal scales and measurement principles. But we note that when any atmospheric model is initialized, the input parameters from various sources are used, which may have different spatial and temporal resolutions and measurement principles. Moreover, datasets from various sources are also utilized in atmospheric models across different parametrization schemes and nudging. In support of isotope tuning, we note that nudging is a well-known technique where the model values are adjusted to accord with the observed values. For example, Graf et al. (2019) used point-based radiosonde RH and T observations, as well as isotope outputs from a limited-area model (Pfahl et al., 2012; Villiger et al., 2023), with a km-scale resolution. These two datasets have different scales and measurement principles. Guided by their argument, we have taken the average Radiosonde profiles of each sampling day as our choice and adjusted the lowermost parts to match the measured RH and T values at the ground taken from the IMD.

(c) The isotope profiles were constructed initially using ground observations as boundary values. However, this resulted in a mismatch with the observed values in Run-2, and we had to tune to lower dD values and higher $\delta^{18}O$ values (and consequently lower d-excess values) to achieve good agreement. It should be mentioned here that Risi et al. (2023) discussed a similar idea in their study of water isotopes in tropical squall lines; they indicated that convective downdrafts can introduce depleted vapour produced by rain re-evaporation in the boundary layer. Another limitation is that the vapour samples were collected for a duration of about a few hours, which did not coincide exactly with the 24-h rain collection period.

(d) The raindrop formation height was assumed to be the CLWC peak level for all rainy days, and the drops were all introduced at that level. However, it is well known that raindrops do not all form at the same height, even on a single day. With the single height assumption for drop introduction, we are neglecting alterations in isotope ratios produced inside the cloud by various microphysical processes.

(e) Although some studies pointed out that collision-coalescence is an important warm rain process that occurs in the Western Ghat regions of India (Konwar et al., 2014) we did not include it in the model. Since the BCIM follows evolution of a single droplet there is no opportunity for collision coalescence, and we have to rely on input droplet diameter being representative of droplet sizes that would occur through collision-coalescence processes. In theory this is all built into the Marshall-Palmer relationship.

(f) The uncertainty values for δD_{rain} is 3.5 ‰, for $dexcess_{rain}$ it is 1.7 ‰, and for drop evaporation it is 8.9%. Several assumptions are required to calculate the uncertainties in these parameters (details are given in the Supplementary Information) and some of them (like linear dependence assumption in multiple regression) may be open to questions.

4.8~~5.3~~ Impact of evaporation on rainfall and heat budget

Formatted: English (India)

Formatted: Indent: Left: 0 cm, Hanging: 0.63 cm

Presence of evaporation of raindrops during the Indian Summer Monsoon has been postulated earlier in several theoretical models, but this study provides, for the first time, a quantitative estimate of rain evaporation on a day-to-day basis in the monsoon season using combined rain and vapour isotope data in a below cloud interaction model. We found that about 235 % raindrop evaporation occurred in 2019 monsoon season in the highly humid Pune region. The average seasonal rainfall in Pune is about 55 cm (during monsoon), and if ~235 % of this is evaporated, it would mean considerable cooling of the boundary layer, leading to localized downdrafts, formation of cold pools, and changes in atmospheric stability. Cooling can also hinder efficient formation of convection (Hwong and Muller, 2024) and can have a large effect on the precipitation patterns in the tropics (Bacmeister et al., 2006; Sarkar et al., 2023). Given the large share of precipitation recycling found in this study for Pune, the question arises as to~~:~~ how large ~~is the precipitation~~the precipitation recycling ~~at~~ is at larger scales, i.e., regional or continental ~~scales, as~~scales ~~well as in other seasons over India~~. We need to have a comprehensive program for carrying out such analysis, aided with appropriate BCIM input parameters, to understand the evaporation of raindrops over various climatic subdivisions in India. Moreover, high-frequency observation of vapour and rain isotopes would be useful to quantify this fraction during various convective events associated with low-pressure systems during the monsoon. A quantitative estimate of raindrop evaporation would be of great help in modelling the energy and moisture budget during the monsoon season.

Formatted: Font: Not Bold, Font color: Auto, Condensed by 1.2 pt

Formatted: No bullets or numbering

Formatted: Indent: First line: 0 cm

~~5 Summary and Conclusions~~

5.~~5.1~~ ~~Key Findings~~Conclusions

(1) This study reveals substantial temporal variability in atmospheric vapour isotopes in Pune during the 2019 monsoon, with $\delta^{18}O$ ranging from −19.2‰ to −9.4‰ and δD from −123.7‰ to −63.4‰. Rain isotopes show comparatively smaller variability ($\delta^{18}O$: −7.5‰ to 1.2‰; δD: −58.9‰ to 11.8‰).

(2) Four events of markedly depleted rain and vapour isotopes were identified, coinciding with negative outgoing longwave radiation (OLR) anomalies and high rainfall indicative of strong convection and effect of Rayleigh condensation. These events likely reflect uplift of moist air parcels to higher altitudes (~5.5 km), ~~where isotopically depleted vapour dominates. Evidence from a second peak in the cloud liquid water content supports this mechanism.~~and condensation to droplets during ascent following Rayleigh distillation.

(3) Vapour isotope data shows a distinct seasonal trend, with increasing vapour d-excess and slightly decreasing $\delta^{18}O$ after mid-August, particularly in September. The strong anti-correlation between vapour $\delta^{18}O$ and d-excess at the ground suggests increasing contributions from evaporative sources over time. Downdrafted vapour with potential contribution from raindrop evaporation possibly constitutes one such source.

(4) $\Delta\delta$–Δd analysis further confirms the importance of sub-cloud evaporation, with ~50% of data points falling in the evaporation-dominated quadrant. The derived slope (−0.45) indicates stronger

evaporation compared to mid-latitude systems, consistent with higher temperatures (~25°C) in Pune enhancing kinetic fractionation effects.

(5) To quantify the sub-cloud processes altering the rain isotope values, we used the Below Cloud Interaction Model BCIM. Upon reasonable tuning of the input parameters, we obtained good agreement between the observed and model rain isotope values at the ground level. Using the model, raindrop evaporation is quantified on daily scale, revealing an average mass loss of ~23% (range: 4–61%) in the sub-cloud layer. Excluding extreme cases, evaporation averages 18 ± 8%, highlighting substantial modification of rain isotopes.

(6) Rain drop evaporation can reduce the rainfall substantially especially during low precipitation (less than 10 mm/day). The average seasonal evaporation means considerable cooling of the boundary layer, leading to localized downdrafts, formation of cold pools, and changes in atmospheric stability hindering efficient formation of convection.

~~We analysed isotope ratios of daily rain and atmospheric vapour samples collected from the surface level at Pune, a tropical rain shadow region in Western India, during the summer monsoon season (June-early October) of 2019. The seven major findings of our study are listed below:~~

~~1. The vapour isotopes show considerable temporal variation (with $\delta^{18}O$ from -19.2 ‰ to -9.4 ‰ and δD from -123.7‰ to -63.4‰). The corresponding rain isotope variations are smaller, $\delta^{18}O$ from -7.5 ‰ to 1.2 ‰ and δD from 58.9‰ to 11.8‰. The rain isotopes are not in equilibrium with the ground vapour. In most cases, the rain $\delta^{18}O$ values are higher than expected from equilibrium with the ground vapour (by about 2‰ on average). In contrast, the δD values are only a little higher, on average, by about 0.7‰; but there are some extreme values, some are higher by about 20 ‰ and some are lower by about 15‰. The deviation from equilibrium is caused by fractionation that raindrops suffer through evaporative exchange (involving equilibrium and kinetic fractionations) during their fall. This fractionation changes the isotope ratios of droplets that originated at heights of 830 ±70 mbar.~~

~~Interestingly, considering the whole monsoon season of 2019, there were four events extending over a few days when both rain and vapour isotope ratios were considerably lower (for example, rain values were less than the mean – 0.5 standard deviation, with $\delta^{18}O$ less than -2.6 ‰). These events seem to be related to regional meteorological characteristics (see below).~~

~~2. We note that the low rain isotope events are synchronous with negative OLR anomalies. Negative OLR anomalies during the Indian summer monsoon are usually associated with large-scale convections (Sengupta et al., 2020). The intense convective events, indicated by these anomalies, lift the air parcels to higher altitudes where the ambient vapour isotope ratios are highly depleted. Droplets formed from these vapours are correspondingly depleted. The drop isotope values may be so negative that even evaporative exchanges may not alter/increase their values much, especially if they are of big size. The high negative isotope values of ground vapours could be due to downdrafts associated with strong evaporative cooling of raindrops. The proposition that air parcels are lifted to higher altitudes during intense convective events is supported by the presence of a second~~

Formatted: Font: Not Bold

Formatted: Indent: Left: 0 cm, Hanging: 1.27 cm

Formatted: Indent: Left: 0 cm

Formatted: Indent: Left: 0 cm, First line: 0 cm

Formatted: No bullets or numbering

Formatted: Indent: Left: 0 cm

Formatted: No bullets or numbering

~~CLWC peak (about 550 mb; see Fig. 3) for 19, 25, 27 Sept, 2019 when the rain and vapour isotopes were both highly depleted (rain δD values are -39 ‰, -49 ‰ and -59 ‰ compared to the average of -7‰) and associated with the negative OLR anomaly (Fig. 2). It seems that on those days intense convection lifted the moist air parcels to about 5.5 km which were responsible for high second CLWC peaks.~~

Formatted: Indent: Left: 0 cm

~~3. A gradual increase in the d-excess values of vapour and a small but notable decrease in $\delta^{18}O$ values in the later part of the monsoon (after mid-August) are observed. The high vapour d-excess in September is especially noticeable. We also find a strong anti-correlation between vapour $\delta^{18}O$ and vapour d-excess values. Such anti-correlation usually indicates a significant contribution to the ground vapour from evaporative sources, which, in our case, accumulated slowly with the progress of the monsoon. Pathak et al. (2014) also found a higher precipitation recycling ratio, that is, the ratio of recycled precipitation to total precipitation in central India, at the end of the monsoon (September). In contrast, the rain d-excess values are not significantly different because there is no such cumulative effect for the rain.~~

Formatted: No bullets or numbering

~~4. The above observations suggest increased vapour contribution from evaporation of raindrops and/or from local evapotranspiration (ET) sources, especially increasing with the monsoon progress. However, vapour supply from surface sources cannot be a large factor. Pathak et al. (2014) showed that for central India, the ET contribution increases with the progress of the Monsoon but can at best account for 5 to 10% of the vapour mass. Therefore, we strongly believe that the downdraft of depleted vapour (and not local supply) is the main source of low $\delta^{18}O$ (and high d-excess) surface vapour (Risi et al., 2023). The depleted vapour in the sub-cloud region can originate from raindrop evaporation, and such vapour can be downdrafted by the drag of the falling raindrops. However, a single-column model like BCIM cannot capture this process.~~

~~5. In the $\Delta\delta$-Δd (Δ indicates the isotope ratio of vapour in equilibrium with rain minus the ambient vapour isotope ratio, following Graf et al., 2019) cross plot, about half of the data points lie in the lower right quadrant, which signifies the importance of raindrop evaporation over Pune and the adjoining region during our study period. The distribution of points in this quadrant is indicative of drop evaporation, but this fact alone cannot quantify the magnitude. We determined the slope $\Delta d/\Delta\delta$ of the points in the cross plot and found a value of -0.45, which suggests that the evaporation in Pune was intense. This is because a higher slope in the cross plot is caused by a relatively magnified effect of d-excess difference between the rain (and corresponding equilibrated vapour) and the ambient vapour caused by a larger evaporation. A comparison can be made with the study of Graf et al. (2019), who found a lower slope at a value of -0.31 for Zurich. The slope is essentially due to a differential effect in evaporative fractionation. Evaporation decreases rain d-excess but increases rain δD. However, the magnitudes of changes, negative for d-excess and positive for δD, are not the same. Fractionation values (involving equilibrium and kinetic factors) show that the change in δD is larger and that in d-excess is lower (about 30% of the δD change, considering only the absolute values for the changes). This is because in evaporation, the kinetic effect operates in addition to the equilibrium fractionation and that has more influence on δD compared to $\delta^{18}O$.~~

Formatted: Indent: Left: 0 cm

~~The factors that influence evaporation are RH, T and drop diameter. As mentioned before, their relative influence is expressed by a multiple regression equation (EQ. 2) using the normalized values of the variables. If~~

~~the evaporation is higher (due to higher temperature and lower RH) the deviation from the equilibrium fractionation will be more, and the slope will be higher (Gat, 1996). In the frontal systems of Switzerland, the temperature was about 12°C and RH about 80% (Graf et al., 2019) compared to Pune, where T was about 25° C and RH about 85%. Since we know that temperature plays an important role (as much as RH) for evaporation (see coefficients of the normalized evaporation equation, 0.370 against 0.329 in the multiple regression equation (EQ. 2)), we expect more evaporation for the large increase in Pune temperature, we expect more evaporation. This factor possibly leads to a higher slope value of 0.45 for Pune compared to 0.31 for Zurich.~~

~~6. To quantify the sub-cloud processes altering the rain isotope values, we used the Below Cloud Interaction Model BCIM. Upon reasonable tuning of the input parameters, we obtained a notable agreement between the observed and model rain isotope values at the ground level.~~

~~7. Since the BCIM is found to be applicable to our study area, we estimate the raindrop evaporation parameter from the model output. An event-to-event quantification of raindrop evaporation is the key finding of our study. The model gives a net reduction of the drop mass at the ground level, and we can define the relative reduction ($1-m/m_o$) as a measure of the effective rain evaporation. Using this innovative technique, the model shows that, on average, about 23 % (varying from 4 % to 60 %) of the drop mass evaporates in the sub-cloud layer. There are four abnormally large values (46, 48, 58, and 60 %) of evaporation. The largest value is probably due to low RH (~78%) and high temperature on that day, but as for the other days, probably a combination of smaller drop size and lower RH played a role. Excluding these four values, the average evaporation is 18±8 % (range of 4 to 30 %).~~

~~5.2 Limitations and uncertainty of the derived parameters~~

~~The isotope technique and the BCIM, which we used, are associated with the following limitations:~~

~~(a) We used TES satellite data averaged over 2005-2009 to guide our choice of vapour isotope profiles, but the year of analysis was 2019. In this matter, there is no way to ascertain the degree of deviation of the true profile from the adopted ones in Run-2 and in Run-3.~~

~~(b) There are limitations on the use of RH and T from radiosonde. On operating days, the radiosondes are usually launched at 00Z and 1200Z in Pune. Due to operational challenges, these measurements are not generally carried out when there is rain. The radiosonde data for Pune are expected to be reasonable for use in the model if we can at least show that the difference between the two consecutive available measurements is not large. The difference between RH (ΔRH) and temperature (ΔT) measured at 1200Z and 00Z is plotted against height in Fig. SI-12-1 for the 29 days that are considered in the BCIM runs. The figure shows that the ΔRH values are within ± 10% on most days (~80% of the total sampling days) and ΔT values are within 2°C. This is expected as those parameters over western India do not vary much during the Indian Summer Monsoon (Pathak et al, 2014). We need to check how serious these differences are in the context of their use in the model. We have shown through sensitivity analyses and two multiple regression analyses that the effects of the daily scale variation in RH and T on model rain isotope values and evaporation fraction are not significant. We also demonstrate further that the RH and T data from~~

Formatted: No bullets or numbering

Formatted: Indent: Left: 0 cm

Formatted: No bullets or numbering

Formatted: Body Text, Justified, Right: -0.08 cm, Space Before: 0.05 pt, Line spacing: Multiple 1.52 li

the radiosonde used in this study is more reliable than the same obtained from any satellite datasets.

The $\delta^{18}O$ profiles were adopted based on the δD and $\delta^{18}O$ profiles obtained from the LMDZ model. As noted, this did not give us good agreement with the observations. Run-2 uses radiosonde for the thermodynamic profile, δD from satellite data from 2005-2009, and $\delta^{18}O$ from the d-excess of the GCM extrapolated to the observed vapour measurement at the ground. We realize that there are major concerns with these inputs coming from different data products that all have different spatial/temporal scales and measurement principles. But we would like to emphasize that when any atmospheric model is initialised, by necessity, the input parameters from various sources are used, which may have different spatial and temporal resolutions and measurement principles. Moreover, datasets from various sources are also utilized in the atmospheric model across different parametrization schemes and nudging. Nudging is a well-known technique where the model values are adjusted to accord with the observed values, where available. For example, Graf et al. (2019) used point based radiosonde RH and T observations, as well as isotope outputs from a limited area model (Pfahl et al., 2012; Villiger et al., 2023), with a km scale resolution, as input to BCIM. These two datasets have different scales and measurement principles. Guided by their argument, we have taken the Radiosonde profiles of each sampling day as our choice and adjusted the lowermost parts to match the measured RH and T values at the ground taken from the IMD.

(c) The isotope profiles were constructed using ground observations as boundary values. However, this also resulted in a mismatch with the observed values (in Run-2), and we had to tune to lower $\delta^{18}O$ values and higher d-excess values to achieve good agreement. It should be mentioned here that Risi et al. (2023) also discussed a similar idea in their study of water isotopes in tropical squall lines, that convective downdrafts can introduce depleted vapour produced by rain re-evaporation in the boundary layer. Another limitation is that the vapour samples were collected for a duration (about a few hours) that did not coincide exactly with the longer rain collection period (about 24 hours).

(d) The raindrop formation height was assumed to be the CLWC peak level for all rainy days, and the drops were all introduced at that level. However, it is well known that raindrops do not all form at the same height, even on a single day. With this assumption, we are neglecting alterations in isotope ratios produced inside the cloud by various microphysical processes.

(e) Although some studies pointed out that collision coalescence is an important warm rain process that occurs in various rain shadow regions of India (Padmakumari et al., 2024), including those in the Western Ghats (Konwar et al., 2014), BCIM neglects the process while estimating rain isotope values. We think that this may introduce some error in rain evaporation estimation, but that cannot be quantified in the present study. Since collision coalescence is a non-fractionating process, the effect would be only through drop size modification. Therefore, the isotope effect would be a secondary effect and is expected to be small.

(f) We provide uncertainty estimates of the model rain isotope values (δD_{rain}, $dexcess_{rain}$) in section 3.2.3.3 and raindrop evaporation fractions in section 4.3. Several assumptions are required to

~~calculate the uncertainties in these parameters. The uncertainty values for δD_{rain} is 3.5 ‰, for $dexcess_{rain}$ it is 2 ‰, and for drop evaporation it is 10%.~~

~~**5.3 Impact of evaporation on rainfall and heat budget**~~

~~Presence of evaporation of raindrops during the Indian Summer Monsoon has been postulated earlier in several theoretical models, but this study provides, for the first time, a quantitative estimate of rain evaporation on a day-to-day basis in the monsoon season using combined rain and vapour isotope data. We found that about 25 % raindrop evaporation occurred in 2019 monsoon season in the highly humid Pune region. The average seasonal rainfall in Pune is about 55 cm (during monsoon), and if ~25 % of this is evaporated, it would mean considerable cooling of the boundary layer, leading to localized downdrafts, formation of cold pools, and changes in atmospheric stability. Cooling can also hinder efficient formation of convection (Hwong and Muller, 2024) and can have a large effect on the precipitation patterns in the tropics (Baemeister et al., 2006; Sarkar et al., 2023). Given the large share of precipitation recycling found in this study for Pune, the question arises: how large is the precipitation recycling at larger scales, i.e., regional or continental scales, as well as in other seasons over India. We need to have a comprehensive program for carrying out such analysis, aided with appropriate BCIM input parameters, to understand the evaporation of raindrops over various climatic subdivisions in India. Moreover, high frequency observation of vapour and rain isotopes would be useful to quantify this fraction during various convective events associated with low pressure systems during the monsoon. A quantitative estimate of raindrop evaporation would be of great help in modelling the energy and moisture budget during the monsoon season.~~

Data Availability

Observed rain and vapour isotope data are available upon communication with the corresponding author. The upper-air radiosonde measurements were obtained from the University of Wyoming repository (http://weather.uwyo.edu/upperair/sounding.html). The daily gridded data (zonal and meridional wind, specific humidity, air temperature, and cloud liquid water content) are available from the European Centre for Medium-Range Weather Forecasts Reanalysis (ERA-5; https://www.ecmwf.int/en/forecasts/datasets/reanalysis-datasets/era5). The rainfall data (cumulated over 24 hours) are obtained from the Pune observatories of the IMD (available at the National Data Centre (www.imdpune.gov.in/ndc_new/ndc_index.html)). Apart from daily rainfall, hourly rainfall data and daily average temperature and relative humidity data for the Pune observatory were also obtained from the IMD using the above link. The datasets for 48 h air mass back trajectory analysis at 850 mb pressure level are obtained from the NOAA Hybrid Single-Particle Lagrangian Integrated Trajectory (HYSPLIT) model (https://www.ready.noaa.gov/HYSPLIT.php). We received daily outputs of LMDZ isotope-enabled GCMs, which were provided by Dr. Camille Risi by personal communication. The Interpolated Outgoing Longwave Radiation (OLR) data from NOAA (https://psl.noaa.gov/data/gridded/data.olrcdr.interp.html) is used in this study. Tropospheric Emission Spectrometer (TES) Level 2 (Nadir-Lite-Version 6) retrievals of HDO and H_2O profiles for the available period (2005–2007; https://tes.jpl.nasa.gov/tes/data) are used to construct the vapour δD profile.

Author Contribution

SSN carried out all rain and vapour isotopic measurements and part of the data analyses, installed and ran the

model BCIM. SPR analyzed most of the samples to get the isotopic data, performed all controlled runs in the BCIM, and constructed most of the figures. SS conceptualized the scientific plan and methodology and wrote the initial draft of the manuscript. SKB contributed to data analysis and interpretation of model outputs, corrected the manuscript, and provided useful comments and suggestions. NA contributed to data analysis and running of the BCIM.

Code Availability

We carried out data analysis and plots using licensed versions of Microsoft Excel and Python, the latter being freely available from https://www.python.org/downloads/. The code of the model, BCIM, is freely available from https://git.app.uib.no/Harald.Sodemann/bcim.

Competing interests

The authors declare that they have no conflict of interest.

Acknowledgements

The Indian Institute of Tropical Meteorology, Pune (IITM), is fully supported by the Earth System Science Organization (ESSO) of the Ministry of Earth Sciences, India. This work forms part of the Ph.D. thesis of SSN, who thanks IITM for a fellowship. SPR thanks IITM for a research associateship. We thank Director IITM for his constant encouragement. The NASA Langley Research Centre and the Atmospheric Science Data Centre are acknowledged for the TES dataset. A fruitful discussion with Dr. Camille Risi is also acknowledged. We thank Dr. Pallab Roy for helping with the Bootstrap analysis and making several plots.

References

Aemisegger, F., Spiegel, J. K., Pfahl, S., Sodemann, H., Eugster, W., and Wernli, H.: Isotope meteorology of cold front passages: A case study combining observations and modeling, Geophys. Res. Lett., 42, 5652–5660, https://doi.org/10.1002/2015GL063988, 2015.

Bacmeister, J. T., Suarez, M. J., and Robertson, F. R.: Rain re-evaporation, boundary layer–convection interactions, and Pacific rainfall patterns in an AGCM, J. Atmos. Sci., 63, 3383–3403, 2006.

Bhattacharya S.K., K. Froehlich, P. K. Aggarwal, and K. M. KulkarniIsotopic variation in Indian Monsoon precipitation: Records from Bombay and New Delhi, Geophysical Research Letters, 30(24), 2285, doi:10.1029/2003GL018453, 2003

Bonne, J. L., Masson-Delmotte, V., Cattani, O., Delmotte, M., Risi, C., Sodemann, H., and Steen-Larsen, H. C.: The isotopic composition of water vapour and precipitation in Ivittuut, southern Greenland, Atmos. Chem. Phys., 14, 4419–4439, https://doi.org/10.5194/acp-14-4419-2014, 2014.

Brubaker, K. L., Entekhabi, D., and Eagleson, P. S.: Estimation of Continental Precipitation Recycling, J. Climate, 6, 1077–1089, https://doi.org/10.1175/1520-0442(1993)006<1077:EOCPR>2.0.CO;2, 1993.

Chakraborty, S., Sinha, N., Chattopadhyay, R., Sengupta, S., Mohan, P. M., and Datye, A.: Atmospheric controls on the precipitation isotopes over the Andaman Islands, Bay of Bengal, Sci. Rep., 6, 19555, https://doi.org/10.1038/srep19555, 2016.

Crawford, J., Hollins, S. E., Meredith, K. T., and Hughes, C. E.: Precipitation stable isotope variability and subcloud evaporation processes in a semi-arid region, Hydrol. Process., 31, 20–34, https://doi.org/10.1002/hyp.10885, 2017.

1309 Dai, Q., Yang, Q., Han, D., Rico-Ramirez, M. A., and Zhang, S.: Adjustment of Radar-Gauge Rainfall
1310 Discrepancy Due to Raindrop Drift and Evaporation Using the Weather Research and Forecasting Model and
1311 Dual-Polarization Radar, Water Resour. Res., 55, 9211–9233, https://doi.org/10.1029/2019WR025517, 2019.

1312 Dansgaard, W.: Stable isotopes in precipitation, Tellus A: Dynamic Meteorology and Oceanography, 16, 436,
1313 https://doi.org/10.3402/tellusa.v16i4.8993, 2012.

1314 Deshpande, R. D., Maurya, A. S., Kumar, B., Sarkar, A., and Gupta, S. K.: Rain-vapor interaction and vapor
1315 source identification using stable isotopes from semiarid western India, J. Geophys. Res., 115, 2010JD014458,
1316 https://doi.org/10.1029/2010JD014458, 2010.

1317 Draxler, R. R. and Hess, G.: Description of the HYSPLIT4 modeling system, 1997.

1318 Foote, G. B. and du Toit, P. S.: Terminal Velocity of Raindrops Aloft, J. App. Meteorol. (1962-1982), 8, 249–
1319 253, 1969.

1320 Farrance, I., and Frenkel, R.: Uncertainty of Measurement: A Review of the Rules for Calculating Uncertainty
1321 Components through Functional Relationships, Clin Biochem Rev., 33(2), 49–75, 2012.
1322
1323 Froehlich, K., Kralik, M., Papesch, W., Rank, D., Scheifinger, H., and Stichler, W.: Deuterium excess in
1324 precipitation of Alpine regions – moisture recycling, Isotopes in Environmental and Health Studies, 44, 61–70,
1325 https://doi.org/10.1080/10256010801887208, 2008.

1326 Gat, J. R.: Oxygen and hydrogen isotopes in the hydrologic cycle, Annu. Rev. Earth Planet. Sci., 24, 225–262,
1327 https://doi.org/10.1146/annurev.earth.24.1.225, 1996.

1328 Graf, P., Wernli, H., Pfahl, S., and Sodemann, H.: A new interpretative framework for below-cloud effects on
1329 stable water isotopes in vapour and rain, Atmos. Chem. Phys., 19, 747–765, https://doi.org/10.5194/acp-19-747-
1330 2019, 2019.

1331 Gray, W. M.: Fundamental Importance of Convective Downdrafts and Mass Recycling Within the Tropical
1332 Cloud Cluster and the Typhoon-Hurricane, Trop. Cyclone Res. and Rev., 1, 130–141,
1333 https://doi.org/10.6057/2012TCRR01.14, 2012.

1334 Herman, R. L., Cherry, J. E., Young, J., Welker, J. M., Noone, D., Kulawik, S. S., and Worden, J.: Aircraft
1335 validation of Aura Tropospheric Emission Spectrometer retrievals of HDO / H_2O, Atmos. Meas. Tech., 7, 3127–
1336 3138, https://doi.org/10.5194/amt-7-3127-2014, 2014.

1337 Hersbach, H., Bell, B., Berrisford, P., Hirahara, S., Horányi, A., Muñoz-Sabater, J., Nicolas, J., Peubey, C.,
1338 Radu, R., Schepers, D., Simmons, A., Soci, C., Abdalla, S., Abellan, X., Balsamo, G., Bechtold, P., Biavati, G.,
1339 Bidlot, J., Bonavita, M., De Chiara, G., Dahlgren, P., Dee, D., Diamantakis, M., Dragani, R., Flemming, J.,
1340 Forbes, R., Fuentes, M., Geer, A., Haimberger, L., Healy, S., Hogan, R. J., Hólm, E., Janisková, M., Keeley, S.,
1341 Laloyaux, P., Lopez, P., Lupu, C., Radnoti, G., De Rosnay, P., Rozum, I., Vamborg, F., Villaume, S., and
1342 Thépaut, J.: The ERA5 global reanalysis, Quart. J. Royal Meteorol. Soc., 146, 1999–2049,
1343 https://doi.org/10.1002/qj.3803, 2020.

1344 Hwong, Y.L. and Muller, C.J.: The unreasonable efficiency of total rain evaporation removal in triggering
1345 convective self-aggregation, Geophys. Res. Lett., *51*, p.e2023GL106523.
1346 https://doi.org/10.1029/2023GL106523, 2024.
1347
1348 Ingleby, B., Pauley, P., Kats, A., Ator, J., Keyser, D., Doerenbecher, A., Fucile, E., Hasegawa, J., Toyoda, E.,
1349 Kleinert, T., Qu, W., St. James, J., Tennant, W., and Weedon, R.: Progress toward high-resolution, real-time
1350 radiosonde reports, Bulletin of the American Meteorological Society, 97(11), 2149–2161,
1351 https://doi.org/10.1175/BAMS-D-15-00169.1, 2016
1352
1353 IPCC, A.: Climate change 2014 synthesis report, IPCC: Geneva, Switzerland, 1059–1072, 2014.

1354 Jensen, M. P., Holdridge, D. J., Survo, P., Lehtinen, R., Baxter, S., Toto, T., and Johnson, K. L.: Comparison of
1355 Vaisala radiosondes RS41 and RS92 at the ARM Southern Great Plains site, Atmos. Meas. Tech., 9, 3115–

3129, https://doi.org/10.5194/amt-9-3115-2016, 2016.

Jiang, Y., Yang, L., Li, J., Zeng, Y., Tong, Z., Li, X., and Li, H.: Diurnal variation characteristics of raindrop size distribution observed by a Parsivel2 Disdrometer in the Ili River valley, Adv. in Meteorol. 481661, https://doi.org/10.1155/2024/1481661, 2024.

Konwar, M., Das, S.K., Deshpande, S. M., Chakravarty, K., and Goswami, B. N.: Microphysics of clouds and rain over the Western Ghat, J. Geophys. Res.-Atmos., 119, 6140–6159, https://doi.org/10.1002/2014JD021606, 2014.

Kumar, S., Resmi, E. A., Jash, D., Patade, S., Sumesh, R.K., Andrews, A., Sukumar, N., Aswini, A.R., and Kulkarni, G.: Raindrop size distribution in stratiform precipitation: Insights from spectral bin simulations over the high-altitude cloud physics observatory, Western Ghats. Journal of Atmospheric and Solar-Terrestrial Physics, 277, 106643, 2025

Kumar, S., Hazra, A., and Goswami, B. N.: Role of interaction between dynamics, thermodynamics and cloud microphysics on summer monsoon precipitating clouds over the Myanmar Coast and the Western Ghats, Clim. Dynam., 43, 911–924, https://doi.org/10.1007/s00382-013-1909-3, 2014.

Kumar, T. V. L., Durga, G. P., Rao, K. K., Nagendra, H., and Mall, R. K.: Moisture recycling over the Indian monsoon core region in response to global warming from CMIP5 models, in: Indian Summer Monsoon Variability, Elsevier, 449–466, https://doi.org/10.1016/B978-0-12-822402-1.00008-9, 2021.

Kurita, N.: Water isotopic variability in response to mesoscale convective system over the tropical ocean, J. Geophys. Res.-Atmos., 118, https://doi.org/10.1002/jgrd.50754, 2013.

Law, S.L.G., Kuok, K. K., and Trinidad, S.G.: An Experimental Study on The Correlation of Natural Rainfall Intensities and Raindrop Size Distribution Characteristics, 2021 IOP Conf. Ser.: Mater. Sci. Eng. 1101 012009, 10.1088/1757-899X/1101/1/012009, 2021

Lee, C., Lawson, W. G., Richardson, M. I., Anderson, J. L., Collins, N., Hoar, T., and Mischna, M.: Demonstration of ensemble data assimilation for Mars using DART, MarsWRF, and radiance observations from MGS TES, J. Geophys. Res., 116, E11011, https://doi.org/10.1029/2011JE003815, 2011.

Lee, J. and Fung, I.: Amount effect of water isotopes and quantitative analysis of post-condensation processes, Hydrol. Process., 22, 1–8, https://doi.org/10.1002/hyp.6637, 2008.

Lekshmy, P. R., Midhun, M., Ramesh, R., and Jani, R. A.: ^{18}O depletion in monsoon rain relates to large-scale organized convection rather than the amount of rainfall, Sci. Rep., 4, 5661, https://doi.org/10.1038/srep05661, 2014.

Lekshmy, P. R., Midhun, M., and Ramesh, R.: Influence of stratiform clouds on δD and $\delta^{18}O$ of monsoon water vapour and rain at two tropical coastal stations, J. Hydrol., 563, 354–362, https://doi.org/10.1016/j.jhydrol.2018.06.001, 2018.

Levine, R. C. and Turner, A. G.: Dependence of Indian monsoon rainfall on moisture fluxes across the Arabian Sea and the impact of coupled model sea surface temperature biases, Clim. Dynam., 38, 2167–2190, https://doi.org/10.1007/s00382-011-1096-z, 2012.

Li, X. and Srivastava, R. C.: An Analytical Solution for Raindrop Evaporation and Its Application to Radar Rainfall Measurements, J. Appl. Meteorol., 40, 1607–1616, https://doi.org/10.1175/1520-0450(2001)040<1607:AASFRE>2.0.CO;2, 2001.

Li, X., Tang, C., and Cui, J.: Intra-Event Isotopic Changes in Water Vapor and Precipitation in South China, Water, 13, 940, https://doi.org/10.3390/w13070940, 2021.

Marshall, J. S., and Palmer, W. mcK.: The distribution of raindrops with size, Journal of Meteorology, Shorter contributions, 5, 165-166, 1948

Mandke, S.K., Soman, M. K., and Satyan, V.: Impact of Convective Downdrafts in a GCM on the Simulated Mean Indian Summer Monsoon and its Variability, J. Meteorol. Soc. Jpn, 77, 1061–1082, https://doi.org/10.2151/jmsj1965.77.5_1061, 1999.

Midhun, M., Lekshmy, P. R., Ramesh, R., Yoshimura, K., Sandeep, K. K., Kumar, S., Sinha, R., Singh, A., and Srivastava, S.: The Effect of Monsoon Circulation on the Stable Isotopic Composition of Rainfall, J. Geophys. Res.-Atmos., 123, 5205–5221, https://doi.org/10.1029/2017JD027427, 2018.

Moerman, J. W., Cobb, K. M., Adkins, J. F., Sodemann, H., Clark, B., and Tuen, A. A.: Diurnal to interannual rainfall $\delta^{18}O$ variations in northern Borneo driven by regional hydrology, Earth Planet. Sci. Lett., 369–370, 108–119, https://doi.org/10.1016/j.epsl.2013.03.014, 2013.

Morrison, H., van Lier-Walqui, M., Fridlind, A. M., Grabowski, W. W.,Harrington, J. Y., Hoose, C., et al.: Confronting the challenge ofmodeling cloud and precipitationmicrophysics. Journal of Advances inModeling Earth Systems, 12, e2019MS001689. https://doi.org/10.1029/2019MS001689, 2020.

Munksgaard, N. C., Zwart, C., Haig, J., Cernusak, L. A., and Bird, M. I.: Coupled rainfall and water vapour stable isotope time series reveal tropical atmospheric processes on multiple timescales, Hydrol. Process., 34, 111–124, https://doi.org/10.1002/hyp.13576, 2020.

Murali Krishna, U. V., Das, S. K., Sulochana, E. G., Bhowmik, U., Deshpande, S. M., and Pandithurai, G.: Statistical characteristics of raindrop size distribution over the Western Ghats of India: wet versus dry spells of the Indian summer monsoon, Atmos. Chem. Phys., 21, 4741–4757, https://doi.org/10.5194/acp-21-4741-2021, 2021.

Naik, M,, Jadhav, A. V., Mukhim, S., Kumar, P. P., and Rohini, L.: Bhawar-Cloud base height variability observed using a Laser- Based Ceilometer over a tropical station Pune, India International Journal of Remote Sensing, 45, https://doi.org/10.1080/01431161.2024.2402003, 2003.

Nimya, S. S., Sengupta, S., Parekh, A., Bhattacharya, S. K., and Pradhan, R.: Region-specific performances of isotope enabled general circulation models for Indian summer monsoon and the factors controlling isotope biases, Clim. Dynam., 59, 3599–3619, https://doi.org/10.1007/s00382-022-06286-1, 2022.

Noone D.: Pairing Measurements of the Water Vapor Isotope Ratio with Humidity to Deduce Atmospheric Moistening and Dehydration in the Tropical Mid-troposphere, Journal of climate, 25(13), 4476-4494, https://doi.org/10.1175/JCLI-D-11-00582.1, 2012.

Padmakumari, B., Maheskumar, R. S., Morwal, S.B., and Kulkarni, J. R.: Variability of Index of Coalescence Activity (ICA) over a rain-shadow region during monsoon and its role in cloud seeding programs in India, Atmospheric Research, 304, 107390, 2024

Pathak, A., Ghosh, S., and Kumar, P.: Precipitation Recycling in the Indian Subcontinent during Summer Monsoon, J. Hydrometeorol., 15, 2050–2066, https://doi.org/10.1175/JHM-D-13-0172.1, 2014.

Pattanaik, D., Mandal, R., Dey, A., Phani, R., Chattopadhyay, R., Joseph, S., Sahai, A., and Mohapatra, M.: Extended Range Forecast (ERF) During Southwest Monsoon 2019, 2019.

Pfahl, S., Wernli, H., and Yoshimura, K.: The isotopic composition of precipitation from a winter storm – A case study with the limited-area model $COSMO_{iso}$, Atmos. Chem. Phys., 12, 1629–1648, https://doi.org/10.5194/acp-12-1629-2012, 2012.

Pradhan, R., Singh, N., and Singh, R. P.: Onset of summer monsoon in Northeast India is preceded by enhanced transpiration, Sci. Rep., 9, 18646, https://doi.org/10.1038/s41598-019-55186-8, 2019.

Pranindita, A., Wang-Erlandsson, L., Fetzer, I., and Teuling, A. J.: Moisture recycling and the potential role of forests as moisture source during European heatwaves, Clim. Dynam., 58, 609–624, https://doi.org/10.1007/s00382-021-05921-7, 2022.

Pruppacher, H. R., and Klett, J. D.: Microstructure of Atmospheric Clouds and Precipitation, in: Microphysics of Clouds and Precipitation, vol. 18, Springer Netherlands, Dordrecht, 10–73, https://doi.org/10.1007/978-0-306-48100-0_2, 2010.

Rahul, P., Ghosh, P., Bhattacharya, S.K., and Yoshimura, K.: Controlling factors of rainwater and water vapor isotopes at Bangalore, India: Constraints from observations in 2013 Indian monsoon, J. Geophys. Res.-Atmos., 121, https://doi.org/10.1002/2016JD025352, 2016.

Rajaveni, S. P., Nimya, S. S., Sengupta, S., Datye, A., and Sarma, D.: Three Years of Stable Water Isotope Data of Daily Rain Samples Collected from Three Geomorphic Regions of India, Sci. Data, 11, 1445, https://doi.org/10.1038/s41597-024-04308-7, 2024.

Rao, Y.P.: Southwest Monsoon, Meteorological Monograph Synoptic Meteorology No.1., India Meteorological Department, 1976.

Risi, C., Bony, S., and Vimeux, F.: Influence of convective processes on the isotopic composition (δ^{18}O and δD) of precipitation and water vapor in the tropics: 2. Physical interpretation of the amount effect, J. Geophys. Res., 113, 2008JD009943, https://doi.org/10.1029/2008JD009943, 2008.

Risi, C., Bony, S., Vimeux, F., and Jouzel, J.: Water-stable isotopes in the LMDZ4 general circulation model: Model evaluation for present-day and past climates and applications to climatic interpretations of tropical isotopic records, J. Geophys. Res.-Atmos., 115, https://doi.org/10.1029/2009JD013255, 2010.

Risi, C., Galewsky, J., Reverdin, G., and Brient, F.: Controls on the water vapor isotopic composition near the surface of tropical oceans and role of boundary layer mixing processes, Atmos. Chem. Phys., 19, 12235–12260, https://doi.org/10.5194/acp-19-12235-2019, 2019.

Risi, C., Muller, C., and Blossey, P.: Rain Evaporation, Snow Melt, and Entrainment at the Heart of Water Vapor Isotopic Variations in the Tropical Troposphere, According to Large-Eddy Simulations and a Two-Column Model, J. Adv. Model Earth Syst., 13, e2020MS002381, https://doi.org/10.1029/2020MS002381, 2021.

Risi, C., Muller, C., Vimeux, F., Blossey, P., Védeau, G., Dufaux, C., and Abramian, S.: What Controls the Mesoscale Variations in Water Isotopic Composition Within Tropical Cyclones and Squall Lines? Cloud Resolving Model Simulations in Radiative-Convective Equilibrium, J. Adv. Model Earth Syst., 15, e2022MS003331, https://doi.org/10.1029/2022MS003331, 2023.

Ryu, S., Song, J. J., and Lee, G. W.: Radar–Rain Gauge Merging for High-Spatiotemporal-Resolution Rainfall Estimation Using Radial Basis Function Interpolation, Remote Sens. 17(3), 530; https://doi.org/10.3390/rs17030530, 2025

Salamalikis, V., Argiriou, A. A., and Dotsika, E.: Isotopic modeling of the sub-cloud evaporation effect in precipitation, Sci. Total Environ., 544, 1059–1072, https://doi.org/10.1016/j.scitotenv.2015.11.072, 2016.

Sapucci, L. F., Machado, L. A. T., Da Silveira, R. B., Fisch, G., Monico, J. F. G.: Analysis of Relative Humidity Sensors at the WMO Radiosonde Intercomparison Experiment in Brazil, Journal of Atmospheric And Oceanic Technology, 22, 664-678, 2005.

Saranya, P., Krishan, G., Rao, M. S., Kumar, S., and Kumar, B.: Controls on water vapor isotopes over Roorkee, India: Impact of convective activities and depression systems, J. Hydrol., 557, 679–687, https://doi.org/10.1016/j.jhydrol.2017.12.061, 2018.

Sarkar, M., Bailey, A., Blossey, P., de Szoeke, S. P., Noone, D., Quiñones Meléndez, E., Leandro, M. D., and Chuang, P. Y.: Sub-cloud rain evaporation in the North Atlantic winter trade winds derived by pairing isotopic data with a bin-resolved microphysical model, Atmos. Chem. Phys., 23, 12671–12690, https://doi.org/10.5194/acp-23-12671-2023, 2023.

Sengupta, S., Bhattacharya, S. K., Parekh, A., Nimya, S. S., Yoshimura, K., and Sarkar, A.: Signatures of monsoon intra-seasonal oscillation and stratiform process in rain isotope variability in northern Bay of Bengal and their simulation by isotope enabled general circulation model, Clim. Dynam., 55, 1649–1663,

https://doi.org/10.1007/s00382-020-05344-w, 2020.

Sengupta, S., Bhattacharya, S. K., Sunil, N. S., and Sonar, S.: Quantifying Raindrop Evaporation Deficit in General Circulation Models from Observed and Model Rain Isotope Ratios on the West Coast of India, Atmosphere, 14, 1147, https://doi.org/10.3390/atmos14071147, 2023.

Sinha, N. and Chakraborty, S.: Isotopic interaction and source moisture control on the isotopic composition of rainfall over the Bay of Bengal, Atmos. Res., 235, 104760, https://doi.org/10.1016/j.atmosres.2019.104760, 2020.

Sodemann, H., Aemisegger, F., Pfahl, S., Bitter, M., Corsmeier, U., Feuerle, T., Graf, P., Hankers, R., Hsiao, G., Schulz, H., Wieser, A., and Wernli, H.: The stable isotopic composition of water vapour above Corsica during the HyMeX SOP1 campaign: insight into vertical mixing processes from lower-tropospheric survey flights, Atmos. Chem. Phys., 17, 6125–6151, https://doi.org/10.5194/acp-17-6125-2017, 2017.

Stewart, M. K.: Stable isotope fractionation due to evaporation and isotopic exchange of falling waterdrops: Applications to atmospheric processes and evaporation of lakes, J. Geophys. Res., 80, 1133–1146, https://doi.org/10.1029/JC080i009p01133, 1975.

Tao, W., Chen, J., Li, Z., Wang, C., and Zhang, C.: Impact of aerosols on convective clouds and precipitation, Rev. Geophys., 50, 2011RG000369, https://doi.org/10.1029/2011RG000369, 2012.

Trenberth, K. E.: Atmospheric Moisture Recycling: Role of Advection and Local Evaporation, J. Climate, 12, 1368–1381, https://doi.org/10.1175/1520-0442(1999)012<1368:AMRROA>2.0.CO;2, 1999.

Utsav, B., Deshpande, S. M., Das, S. K., and Pandithurai, G.: Statistical Characteristics of Convective Clouds over the Western Ghats Derived from Weather Radar Observations, J. Geophys. Res.-Atmos., 122, https://doi.org/10.1002/2016JD026183, 2017.

Villiger, L., Dütsch, M., Bony, S., Lothon, M., Pfahl, S., Wernli, H., Brilouet, P.-E., Chazette, P., Coutris, P., Delanoë, J., Flamant, C., Schwarzenboeck, A., Werner, M., and Aemisegger, F.: Water isotopic characterisation of the cloud–circulation coupling in the North Atlantic trades – Part 1: A process-oriented evaluation of COSMOiso simulations with EUREC4A observations, Atmos. Chem. Phys., 23, 14643–14672, https://doi.org/10.5194/acp-23-14643-2023, 2023.

Vimeux, F., Tremoy, G., Risi, C., and Gallaire, R.: A strong control of the South American SeeSaw on the intra-seasonal variability of the isotopic composition of precipitation in the Bolivian Andes, Earth and Planet. Sci. Lett., 307, 47–58, https://doi.org/10.1016/j.epsl.2011.04.031, 2011.

Wang, B., Ding, Y., and Sikka, D.: Synoptic systems and weather, The Asian Monsoon, 131–201, 2006.

Wang, R., Gentine, P., Yin, J., Chen, L., Chen, J., and Li, L.: Long-term relative decline in evapotranspiration with increasing runoff on fractional land surfaces, Hydrol. Earth Syst. Sci., 25, 3805–3818, https://doi.org/10.5194/hess-25-3805-2021, 2021.

Wang, S., Zhang, M., Che, Y., Chen, F., and Qiang, F.: Contribution of recycled moisture to precipitation in oases of arid central Asia: A stable isotope approach, Water Resour. Res., 52, 3246–3257, https://doi.org/10.1002/2015WR018135, 2016.

Worden, J., Noone, D., Bowman, K. et al.: Importance of rain evaporation and continental convection in the tropical water cycle, Nature, 445, 528–532, https://doi.org/10.1038/nature05508, 2007.

Worden, J., Noone, D., Galewsky, J., Bailey, A., Bowman, K., Brown, D., Hurley, J., Kulawik, S., Lee, J., and Strong, M.: Estimate of bias in Aura TES HDO/H_2O profiles from comparison of TES and in situ HDO/H_2O measurements at the Mauna Loa observatory, Atmos. Chem. Phys., 11, 4491–4503, https://doi.org/10.5194/acp-11-4491-2011, 2011.

Wu, Y., Gao, J., Zhao, A., Niu, X., Liu, Y., Ratnasekera, D., Gamage, T. P., and Samantha, A. H. R.: One-year continuous observations of near-surface atmospheric water vapor stable isotopes at Matara, Sri Lanka, reveal a

strong link to moisture sources and convective intensity, Atmos. Chem. Phys., 25, 4013–4033, https://doi.org/10.5194/acp-25-4013-2025, 2025.

Xiao, F., Zhu, B., and Zhu, T.: Inconsistent urbanisation effects on summer precipitation over the typical climate regions in central and eastern China, Theor. Appl. Climatol., 143, 73–85, https://doi.org/10.1007/s00704-020-03404-z, 2021.

Xie, X., Evaristo, R., Troemel, S., Saavedra, P., Simmer, C., and Ryzhkov, A.: Radar Observation of Evaporation and Implications for Quantitative Precipitation and Cooling Rate Estimation, J. Atmos. and Ocean. Technol., 33, 1779–1792, https://doi.org/10.1175/JTECH-D-15-0244.1, 2016.

Xing, M., Liu, W., and Hu, J.: A set of methods to quantitatively evaluate the below-cloud evaporation effect on precipitation isotopic composition: a case study in a city located in the semi-arid regions of Chinese Loess Plateau, https://doi.org/10.5194/acp-2020-312, 26 May 2020.

Xu, H., Guo, J., Tong, B., Zhang, J., Chen, T., Guo, X., Zhang, J., and Chen, W.: Characterizing the near-global cloud vertical structures over land using high-resolution radiosonde measurements, Atmos. Chem. Phys., 23, 15011–15038, https://doi.org/10.5194/acp-23-15011-2023, 2023.

Yoshimura, K., Kanamitsu, M., Noone, D., and Oki, T.: Historical isotope simulation using Reanalysis atmospheric data, J. Geophys. Res., 113, 2008JD010074, https://doi.org/10.1029/2008JD010074, 2008.

Zaitchik, B. F., Macalady, A. K., Bonneau, L. R., and Smith, R. B.: Europe's 2003 heat wave: a satellite view of impacts and land–atmosphere feedbacks, Int. J. Climatol., 26, 743–769, https://doi.org/10.1002/joc.1280, 2006.

Zhang, F., Huang, T., Man, W., Hu, H., Long, Y., Li, Z., and Pang, Z.: Contribution of Recycled Moisture to Precipitation: A Modified d-Excess-Based Model, Geophys. Res. Lett., 48, e2021GL095909, https://doi.org/10.1029/2021GL095909, 2021.

Zhu, G., Zhang, Z., Guo, H., Zhang, Y., Yong, L., Wan, Q., Sun, Z., and Ma, H.: Below-Cloud Evaporation of Precipitation Isotopes over Mountains, Oases, and Deserts in Arid Areas, J. Hydrometeorol., 22, 2533–2545, https://doi.org/10.1175/JHM-D-20-0170.1, 2021.